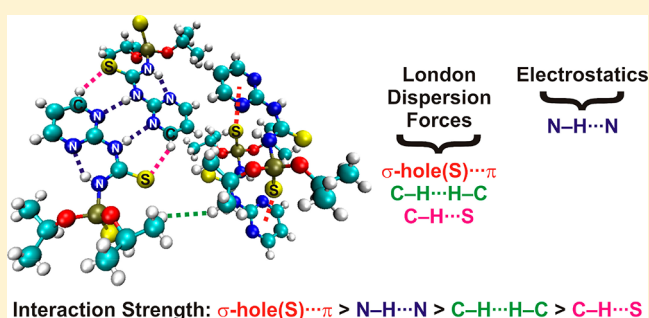


London Dispersion Forces in Crystal Packing of Thiourea Derivatives

Mariusz P. Mitoraj,^{*,†} Maria G. Babashkina,[‡] Alexey Y. Isaev,[§] Yana M. Chichigina,[§] Koen Robeyns,[‡] Yann Garcia,[‡] and Damir A. Safin^{*,‡,§}[†]Department of Theoretical Chemistry, Faculty of Chemistry, Gronostajowa 2, 30-387 Cracow, Poland[‡]Institute of Condensed Matter and Nanosciences, Université Catholique de Louvain, Place L. Pasteur 1, 1348 Louvain-la-Neuve, Belgium[§]Institute of Chemistry, University of Tyumen, Perekopskaya Str. 15a, 625003 Tyumen, Russian Federation

Supporting Information

ABSTRACT: Novel thioureas RNHC(S)NHP(S)(OiPr)₂ [R = (HOCH₂)(Me)₂C (1), Me₂CH₂CH₂ (2), 2-CF₃C₆H₄ (3), 2-Pym (4), and bis-thiourea 1,5-C₁₀H₆{NHC(S)NHP(S)-(OiPr)₂} (5)] have been synthesized and characterized by NMR, X-ray diffraction, Hirshfeld surface analysis, and theoretical ETS-NOCV charge and energy decomposition calculations. The monomers contain multiple intramolecular noncovalent interactions including N–H···X (X = O, 1–3; F, 3; N, 4; S, 5) and C–H···Y (Y = O, 1; N, 2 and 3; S, 4 and 5) augmented further by homopolar C–H···H–C contacts in all the structures. It has been determined that the three-dimensional crystal networks are primarily constituted from intermolecular H···H and H···S contacts due to homopolar C–H···H–C as well as X–H···S (X = N, C) interactions. They are, depending on the system, augmented further by C–H···Y (Y = π, S, F) as well as by σ-hole(S)···π interactions. ETS-NOCV allowed us to delineate that in the case of C–H···H–C, C–H···Y, and σ-hole(S)···π intermolecular interactions, except for the electrostatically dominated N–H···N in 4, London dispersion forces appeared to be a crucial contributor to the stability with non-negligible factors stemming from electrostatics and charge delocalization terms. Remarkably, the dispersion dominated (~50% of the overall stabilization ΔE_{elstat} + ΔE_{orb} + ΔE_{dispersion}) σ-hole(S)···π interactions appeared to be the strongest among all the discovered interactions, including classical hydrogen bonds N–H···N. The electrostatic and charge delocalization contributions within the σ-hole(S)···π interactions amount to ~30% and ~20%, respectively.



INTRODUCTION

London dispersion forces have been recently gaining significant attention in various fields of chemistry, starting from small molecules to end up with large systems in catalysis and material science.^{1,2} It is mostly due to developments of semiempirical dispersion corrections by Grimme.^{3,4} Although they are in principle not as accurate as *ab initio* estimations,^{5,6} it has been proven that they allow researchers to capture and better understand a number of very important physical phenomena and chemical concepts.^{1,2} For example, the recent review by Schreiner and Wagner highlighted the need for “...reconsidering steric effects” since in many cases large bulky hydrophobic substituents, leading to the existence of homopolar C–H···H–C interactions, are truly London dispersion donors which can easily overcompensate for the Pauli (kinetic) repulsion.¹ It leads, for example, to syntheses of extraordinarily stable (>200 °C) dimonido dimers,⁷ formation of bulky tetrahedral nickel complexes,⁸ or even to steering the catalytic activity.⁹ Interestingly, the existence of very short H···H contacts (~1.5 Å) has been first featured theoretically as found, for example, in the recent high quality computational paper by Mandal and co-workers.¹⁰ Firouzi and Shahbazian

have reached even 1.15 Å in rigid hydrocarbons.¹¹ Thereafter, quite similar systems have been isolated experimentally.¹² Furthermore, the azine crystals were also found to be stabilized by C–H···H–C interactions.¹³ It is necessary to point out that although significant progress has been achieved during recent years in understanding the nature of X–H···H–X interactions,^{1–13} there are many known systems where the importance of London dispersion forces has not been yet recognized, as nicely pointed out by Liptrot and Power.² Even more importantly, this subject is still the matter of intensive discussion in the literature especially as far as intramolecular X–H···H–X contacts are taken into account. Here one can list the following disputes on the stability of the biphenyl molecule (planar versus bent),^{14–19} 2-butene isomers,^{20–22} or the nature of intermolecular homopolar B–H···H–B and other similar contacts in hydrogen storage systems.^{23–30}

Apart from the above noncovalent interactions and polar X–H^{δ+}···^{δ-}H–Y (X ≠ Y) bonds,^{31–35} there are other nonconven-

Received: May 22, 2018

Revised: July 10, 2018

Published: July 12, 2018

tional and quite unintuitive weak interactions, which have been discovered during recent years, such as anion $\cdots\pi$ interactions^{36–38} or various types of σ -/ π -hole bonds constituted from the electron deficient regions of molecules and nucleophiles.^{39–43} All these types of weak interactions as well as more classic hydrogen bonds, $\pi\cdots\pi$ stacking, and others are now crucial forces for crystal engineering.^{44–47}

In crystal engineering and growth, the (thio)urea group is of great importance due to the combination of both hydrogen donors arising from the NH groups and the C=O or C=S acceptor centers.^{48–59} Furthermore, modification of the (thio)urea skeleton will make these molecules very attractive. During recent years, our efforts have been directed toward synthesis and understanding various properties of substituted thioureas of the type $R^1R^2NC(S)NHP(X)(OR^3)_2$, where R^1 , R^2 = H, alkyl, aryl; R^3 = *i*Pr, Ph; X = O, S (NTTUs).^{60–90} We have learned that classic hydrogen bonding is crucial for both the structures and properties of NTTUs. Due to recent progress in recognizing novel noncovalent interactions, including homopolar C–H \cdots H–C, we have recently deeply studied a novel set of thiourea derivatives RNHC(S)NHP(S)-(O*i*Pr)₂ by applying bulky hydrophobic R differing in size and accordingly in dispersion donating properties.⁹¹ We have further determined that a significant amount of polar thiourea regions, NH hydrogen donors, thiocarbonyl and thiophosphoryl acceptors, together with large hydrophobic areas, leads to extraordinary stability of the systems arising from the formation of London dispersion dominated nonconventional homopolar dihydrogen C–H \cdots H–C interactions (both intra- and intermolecular) augmented by numerous other contributors (e.g., N–H $\cdots\pi$, N–H \cdots S, N–H \cdots O, C–H \cdots S, C–H $\cdots\pi$, $\pi\cdots\pi$).⁹¹

In this contribution we have decided to study experimentally and theoretically a novel set of sterically demanding NTTUs of the RNHC(S)NHP(S)(O*i*Pr)₂ type, varying in the structure of the substituent at the thiocarbonyl fragment [R = (HOCH₂)(Me)₂C (1), Me₂CH₂CH₂ (2), 2-CF₃C₆H₄ (3), 2-Pym (4)], and bis-thiourea 1,5-C₁₀H₆{NHC(S)NHP(S)(O*i*Pr)₂}₂ (5) (Chart 1), hoping to generate novel architectures driven by synergistic action of multiple types of classic and recently topical noncovalent interactions. We have used herein R ligands containing both hydrophobic and polar regions that shall generate diversity of noncovalent interactions. In order to identify and deeply understand the synergy between different

types of noncovalent interactions responsible for the crystal packing, the Hirshfeld surface analyses^{92–95} as well as DFT-based quantum chemical calculations due to the ETS-NOCV charge and energy decomposition scheme,⁹⁶ will be employed. Additionally, NMR spectroscopy and X-ray diffraction data are used to characterize the obtained thioureas.

METHODS

Physical Measurements. NMR spectra in CDCl₃ were recorded on a Bruker Avance 300 MHz spectrometer. ¹H, ¹⁹F, and ³¹P{¹H} NMR spectra were recorded at 299.948, 282.404, and 121.420 MHz, respectively. Chemical shifts are reported with reference to SiMe₄ (¹H), CFCl₃ (¹⁹F{¹H}), and 85% H₃PO₄ (³¹P{¹H}). Elemental analyses were obtained on a Thermoquest Flash EA 1112 analyzer from CE Instruments.

ETS-NOCV Bonding Analysis. The Natural Orbitals for Chemical Valence (NOCV) ψ_i constitute the canonical representation for a differential density matrix $\Delta\rho$ (it is formed by subtracting the appropriate molecular fragments density matrices from a density matrix of a molecule under consideration) in which $\Delta\rho$ adopts a diagonal form.⁹⁶ It gives rise to the corresponding eigenvalues ν_i and the related vectors ψ_i . NOCVs occur in pairs (ψ_{-i}, ψ_k) related to $|\nu_i|$, and they decompose overall deformation density $\Delta\rho$ into bonding components with different symmetries ($\Delta\rho_k$):

$$\Delta\rho(r) = \sum_{k=1}^{M/2} \nu_k [-\psi_{-k}^2(r) + \psi_k^2(r)] = \sum_{k=1}^{M/2} \Delta\rho_k(r)$$

Usually, a few k allow one to recover a major shape of $\Delta\rho$.⁹⁶ By combining NOCVs with ETS scheme in ETS-NOCV,⁹⁶ one can obtain the related energetics, $\Delta E_{\text{orb}}(k)$, in addition to qualitative picture emerging from $\Delta\rho_k$. ETS originally divides the total bonding energy, between fragments, ΔE_{total} into four distinct components: $\Delta E_{\text{total}} = \Delta E_{\text{elstat}} + \Delta E_{\text{Pauli}} + \Delta E_{\text{orb}} + \Delta E_{\text{dispersion}}$. The ΔE_{elstat} is an energy of quasi-classical electrostatic interaction between fragments. The next term, ΔE_{Pauli} , is responsible for repulsive Pauli interaction between occupied orbitals on the two fragments. The third component, ΔE_{orb} , is stabilizing and shows formation of a chemical bond (including polarizations). In the ETS-NOCV scheme ΔE_{orb} is expressed in terms of the eigenvalues ν_k and diagonal Fock energy matrix elements F_{ii}^{TS} (transformed into NOCV representation) as

$$\Delta E_{\text{orb}} = \sum_k \Delta E_{\text{orb}}(k) = \sum_{k=1}^{M/2} \nu_k [-F_{-k,-k}^{\text{TS}} + F_{k,k}^{\text{TS}}]$$

Finally, $\Delta E_{\text{dispersion}}$ denotes the semiempirical Grimme dispersion correction (D3).^{3,4} The DFT method has been applied with BLYP-D3/TZP.

Synthesis of 1–5. A solution of 2-amino-2-methyl-1-propanol, *N,N*-dimethylethylenediamine, 2-(trifluoromethyl)aniline, 2-aminopyrimidine (5 mmol; 0.446, 0.441, 0.806, or 0.476 g) or 1,5-diaminonaphthalene (2.5 mmol, 0.396 g) in CH₂Cl₂ (15 mL) was treated under stirring with a solution of (*i*PrO)₂P(S)NCS (6 mmol, 1.436 g) in the same solvent. The mixture was stirred for 1 h. The solvent was removed in a vacuum, and the product was purified by recrystallization from a 1:5 (v/v) mixture of CH₂Cl₂ and *n*-hexane.

1. Yield: 1.494 g (91%). ¹H NMR: δ = 1.35 (d, ³J_{H,H} = 6.3 Hz, 12H, CH₃, *i*PrO), 1.45 (s, 6H, CH₃, (HOCH₂)(Me)₂C), 2.75 (br. s, 1H, OH), 3.86 (s, 2H, CH₂, (HOCH₂)(Me)₂C), 4.79 (d. sept, ³J_{POCH} = 10.7 Hz, ³J_{H,H} = 6.3 Hz, 2H, OCH, *i*PrO), 6.72 (br. s, 1H, PNH), 7.91 (s, 1H, alkylNH) ppm. ³¹P{¹H} NMR: δ = 53.1 ppm. Calc. for C₁₁H₂₅N₂O₃PS₂ (328.42): C, 40.23; H, 7.67; N, 8.53. Found: C, 40.34; H, 7.72; N, 8.59%.

2. Yield: 1.375 g (84%). ¹H NMR: δ = 1.33 (t, ³J_{H,H} = 6.4 Hz, 12H, CH₃, *i*PrO), 2.24 (s, 6H, CH₃, Me₂NCH₂CH₂), 2.49 (t, ³J_{H,H} = 6.0 Hz, 2H, CH₂, Me₂NCH₂CH₂), 3.63 (t, ³J_{H,H} = 5.9 Hz, ³J_{H,CNH} = 4.1 Hz, 2H, CH₂, Me₂NCH₂CH₂), 4.78 (d. sept, ³J_{POCH} = 10.6 Hz, ³J_{H,H} = 6.3 Hz, 2H, OCH, *i*PrO), 5.66 (br. s, 1H, PNH), 8.05 (s, 1H, alkylNH) ppm. ³¹P{¹H} NMR: δ = 54.7 ppm. Calc. for

Chart 1. Structural Diagrams of 1–5

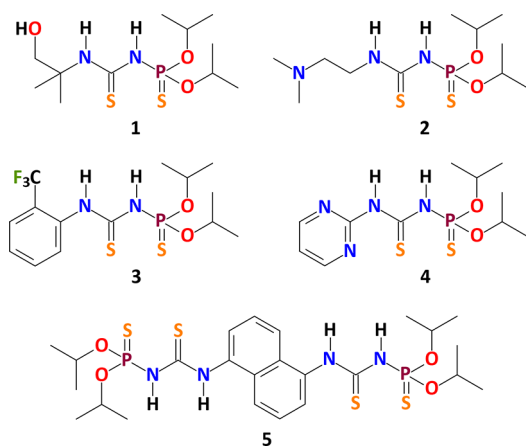


Table 1. Selected Parameters and Structural Data for 1–5

	1	2	3	4	5
empirical formula	C ₁₁ H ₂₅ N ₃ O ₂ PS ₂	C ₁₁ H ₂₆ N ₃ O ₂ PS ₂	C ₁₄ H ₂₀ F ₃ N ₂ O ₂ PS ₂	C ₁₁ H ₁₉ N ₄ O ₂ PS ₂	C ₂₄ H ₃₈ N ₄ O ₄ P ₂ S ₄
formula weight, g mol ⁻¹	328.42	327.44	400.41	334.39	636.76
crystal system	triclinic	monoclinic	triclinic	triclinic	triclinic
space group	$P\bar{1}$	$P2_1/n$	$P\bar{1}$	$P\bar{1}$	$P\bar{1}$
T, K	295(2)	297(2)	150(2)	295(2)	100(2)
a, Å	9.1039(6)	10.0936(8)	8.1513(9)	10.0356(4)	8.139(3)
b, Å	9.5907(8)	16.2214(11)	10.4889(9)	10.1983(12)	9.067(6)
c, Å	10.6186(8)	10.9422(9)	11.8226(6)	10.5711(15)	10.817(8)
α, °	104.764(7)	90.0	105.534(6)	65.429(13)	97.87(6)
β, °	100.494(6)	102.188(8)	94.794(7)	68.473(10)	93.91(4)
γ, °	98.787(6)	90.0	98.396(8)	61.282(10)	106.16(4)
V, Å ³	861.97(11)	1751.2(2)	955.43(14)	843.75(16)	754.7(8)
Z	2	4	2	2	1
ρ	1.265	1.242	1.392	1.316	1.401
μ(Mo–Kα)	0.407	0.398	0.399	0.416	0.458
reflections collected	8444	11027	6407	11456	1583
unique reflections	3020	3238	3278	3267	1583
R _{int}	0.045	0.051	0.035	0.033	0.000
R ₁ (all)	0.0443	0.0433	0.0451	0.0416	0.1891
wR ₂ (all)	0.1168	0.1021	0.0893	0.0957	0.3038

C₁₁H₂₆N₃O₂PS₂ (327.44): C, 40.23; H, 7.67; N, 8.53. Found: C, 40.34; H, 7.72; N, 8.59%.

3. Yield: 1.722 g (86%). ¹H NMR: δ = 1.38 (d, ³J_{H,H} = 6.4 Hz, 6H, CH₃, *i*PrO), 1.41 (d, ³J_{H,H} = 6.4 Hz, 6H, CH₃, *i*PrO), 4.89 (d, sept, ³J_{POCH} = 10.2 Hz, ³J_{H,H} = 6.3 Hz, 2H, OCH, *i*PrO), 7.32 (d, ²J_{HNP} = 10.5 Hz, 1H, PNH), 7.42 (t, ³J_{H,H} = 7.6 Hz, 1H, 4-CH, C₆H₄), 7.60 (t, ³J_{H,H} = 7.6 Hz, 1H, 5-CH, C₆H₄), 7.70 (d, ³J_{H,H} = 7.6 Hz, 1H, 3-CH, C₆H₄), 7.77 (d, ³J_{H,H} = 7.6 Hz, 1H, 6-CH, C₆H₄), 9.42 (s, 1H, arylNH) ppm. ¹⁹F NMR: δ = -62.1 ppm. ³¹P{¹H} NMR: δ = 53.4 ppm. Calc. for C₁₄H₂₀F₃N₂O₂PS₂ (400.41): C, 42.00; H, 5.03; N, 7.00. Found: C, 42.11; H, 5.11; N, 7.07%.

4. Yield: 1.555 g (93%). ¹H NMR: δ = 1.21 (d, ³J_{H,H} = 6.2 Hz, 6H, CH₃, *i*PrO), 1.22 (d, ³J_{H,H} = 6.2 Hz, 6H, CH₃, *i*PrO), 4.55 (d, sept, ³J_{POCH} = 10.4 Hz, ³J_{H,H} = 6.2 Hz, 2H, OCH, *i*PrO), 8.41 (d, ³J_{H,H} = 5.2 Hz, 2H, 4-CH + 6-CH, 2-Pym), 8.71 (t, ³J_{H,H} = 5.2 Hz, 1H, 5-CH, 2-Pym), 8.84 (br. s, 1H, arylNH), 12.71 (br. s, 1H, PNH) ppm. ³¹P{¹H} NMR: δ = 57.3 ppm. Calc. for C₁₁H₁₉N₄O₂PS₂ (334.39): C, 39.51; H, 5.73; N, 16.75. Found: C, 39.42; H, 5.69; N, 16.84%.

5. Yield: 1.305 g (82%). ¹H NMR: δ = 1.22 (d, ³J_{H,H} = 6.2 Hz, 12H, CH₃, *i*PrO), 1.23 (d, ³J_{H,H} = 6.2 Hz, 12H, CH₃, *i*PrO), 4.56 (d, sept, ³J_{POCH} = 10.3 Hz, ³J_{H,H} = 6.2 Hz, 4H, OCH, *i*PrO), 7.20 (br. s, 2H, PNH), 7.54–7.70 (m, 4H, C₁₀H₆), 7.92–8.08 (m, 2H, C₁₀H₆), 9.40 (s, 2H, arylNH) ppm. ³¹P{¹H} NMR: δ = 54.9 ppm. Calc. for C₂₄H₃₈N₄O₄P₂S₄ (636.78): C, 45.27; H, 6.01; N, 8.80. Found: C, 45.36; H, 6.12; N, 8.91%.

Single Crystal X-ray Diffraction. The X-ray data for 1–5 were collected on a Mar345 image plate detector using Mo–K_α radiation (Xenocs Fox3D mirror). The data were integrated with the CrysAlis(Pro) software.⁹⁷ The implemented empirical absorption correction was applied. The structures were solved by SHELXS⁹⁷ and refined by full-matrix least-squares on |F²l, using SHELXL-97.⁹⁸ Non-hydrogen atoms were anisotropically refined, and the hydrogen atoms were placed on calculated positions in riding mode with temperature factors fixed at 1.2 times U_{eq} of the parent atoms and 1.5 times U_{eq} for the methyl groups. The details of crystal structures and refinement are presented in Table 1. Figures were generated using the Mercury program.⁹⁹

RESULTS AND DISCUSSION

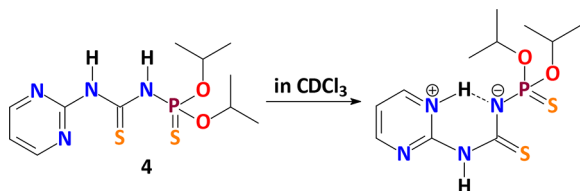
The functionalized thioureas 1–5 (Chart 1) were readily fabricated by addition of the corresponding amine to the solution of isothiocyanate (*i*PrO)₂P(S)NCS in CH₂Cl₂. The

final products are well soluble in dichloromethane, chloroform, acetone, acetonitrile and insoluble in *n*-hexane and water.

The ³¹P{¹H} NMR spectra of the thioureas 1–3 and 5 in CDCl₃ each exhibit a singlet at 53.1–54.9 ppm, which is the characteristic area for neutral NTTUs (X = S).^{60–90} Contrarily, the ³¹P{¹H} NMR spectrum of 4 in the same solvent contains a remarkably low-field shifted singlet at 57.3 ppm. This confirms the deprotonated form of NTTUs (X = S).^{60–90} The ¹H NMR spectra of 1–5 in CDCl₃ each exhibit a unique set of signals. Particularly, the *i*PrO protons were found as a doublet or two doublets or a triplet for the CH₃ protons at 1.21–1.38 ppm and a doublet of septets for the CHO protons at 4.55–4.79 ppm. The spectrum of 1 contains signals for the (HOCH₂)(Me)₂C group: two singlets for the CH₃ and CH₂ protons at 1.45 and 3.86 ppm, respectively, and a broad singlet for the OH proton at 2.75 ppm. The signals for the Me₂NCH₂CH₂ group in 2 were found as a singlet for the CH₃ protons at 2.24 ppm and as two triplets for the CH₂ protons at 2.49 and 3.63 ppm. The aryl protons in the ¹H NMR spectrum of 3 are shown as two triplets and two doublets at 7.42–7.77 ppm, while the pyrimidine protons in the spectrum of 4 are observed as a doublet and a triplet at 8.41 and 8.71 ppm, respectively. The naphthylene protons were shown in the spectrum of 5 as two multiplets at 7.54–7.70 and 7.92–8.08 ppm. Additionally, the spectra of 1–3 and 5 each contain signals for the PNH proton at 5.66–7.32 ppm. However, the same signal in the spectrum of 4 is remarkably low-field shifted and shown at 12.71 ppm. This clearly indicates a strong intramolecular hydrogen bonding between one of the nitrogen atoms of the pyrimidine function and the hydrogen atom of the phosphorylamide fragment. We have determined that this system indeed exhibits the strongest intramolecular N–H⋯N bond as indicated by the NCI (Non Covalent Index) results, shown as a blue disc area of the reduced density gradient (Figure S1 in the Supporting Information). The RNH proton signals are observed at 7.91–9.42 ppm. It has to be noted that the signals for the arylNH proton of 1 and 2 are considerably high-field shifted with respect to the arylNH proton of 3–5.

On the basis of the NMR spectroscopy data, we conclude that **4** is completely in the zwitterionic form in CDCl_3 (Scheme 1). A similar zwitterion formation, based on the

Scheme 1. Zwitterionic Form of **4** in CDCl_3



corresponding NMR spectra, was recently postulated for the *N*-(thio)phosphorylated thiosemicarbazides $\text{NH}_2\text{N}(\text{Me})\text{C}(\text{S})\text{-NHP}(\text{X})(\text{O}i\text{Pr})_2$ and thioureas $2\text{-PyNHC}(\text{S})\text{NHP}(\text{O})(\text{O}i\text{Pr})_2$ ($\text{X} = \text{O}, \text{S}$).^{70,77,84}

The crystal structures of **1** and **3–5** were each solved in the triclinic space group $P\bar{1}$, while the structure of **2** was best solved in the monoclinic space group $P2_1/n$. Notably, the CH_2OH group in **1** is disordered over two positions with a 62.7% to 37.3% ratio, indicated herein as **1-I** and **1-II**, respectively. The crystal structures of **1–5** are shown in Figures 1, 2, 3, 4, and 5, while selected geometrical parameters,

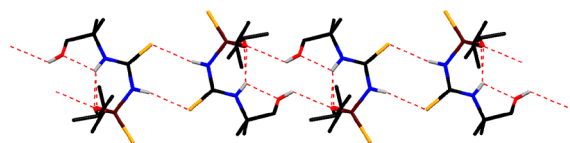


Figure 1. $(\text{P})\text{N}-\text{H}\cdots\text{S}=\text{C}$ H-bonded dimers, linked through the $\text{O}-\text{H}\cdots\text{O}-\text{P}$ H-bonds, in **1** (H atoms not involved in H-bonding are omitted for clarity). Color code: C = black, H = light gray, N = blue, O = red, P = maroon, S = orange.

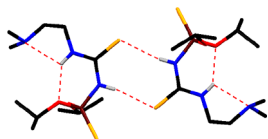


Figure 2. $(\text{P})\text{N}-\text{H}\cdots\text{S}=\text{C}$ P-bonded dimer in **2** (H atoms not involved in H-bonding are omitted for clarity). Color code: C = black, H = light gray, N = blue, O = red, P = maroon, S = orange.

hydrogen bonds, and $\pi\cdots\pi$ stacking are given in Tables 2, 3, and 4, respectively. The geometrical parameters (Table 2) within the SCNPS moiety of all the thioureas are characteristic for NTTUs ($\text{X} = \text{S}$),¹⁰⁰ and differences in the *E* or *Z* conformation of the SCNP and SPNC fragments within the SCNPS backbone can be highlighted (see detail description in the Supporting Information).

To shed more light and to have an in-depth delineation of intermolecular interactions in the reported crystals, we have applied the Hirshfeld surface analysis.^{92–95} The structures of **1-I** and **1-II** were analyzed separately, and as evidenced from the Hirshfeld surface analysis data both structures are very similar with respect to intermolecular interactions. For the sake of brevity, we therefore discuss only **1-I** in detail.

The intermolecular $\text{H}\cdots\text{H}$ contacts (44.0–71.3%) are major contributors to the molecular surface of all the thioureas (Table 5). The alkylamine pendant functions in **1-I** and **2** remarkably increase the proportion of $\text{H}\cdots\text{H}$ contacts. Notably,

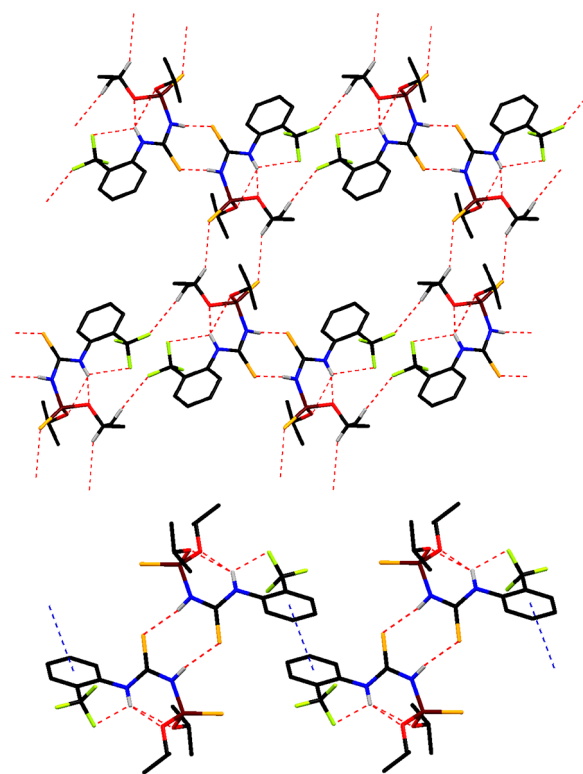


Figure 3. $(\text{P})\text{N}-\text{H}\cdots\text{S}=\text{C}$ H-bonded dimers, linked through the $\text{C}-\text{H}_{i\text{Pr}}\cdots\text{F}-\text{C}$ and $\text{C}-\text{H}_{i\text{Pr}}\cdots\text{S}=\text{P}$ H-bonds (top) and $\pi\cdots\pi$ stacking interactions (bottom), in **3** (H atoms not involved in H-bonding are omitted for clarity). Color code: C = black, H = light gray, N = blue, O = red, P = maroon, S = orange.

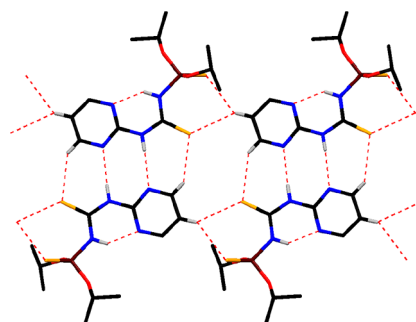


Figure 4. $(\text{Pym})\text{N}-\text{H}\cdots\text{N}_{\text{Pym}}$ and $\text{C}-\text{H}_{\text{Pym}}\cdots\text{S}=\text{C}$ H-bonded dimers, linked through the $\text{C}-\text{H}_{\text{Pym}}\cdots\text{S}=\text{C}$ and $\text{C}-\text{H}_{\text{Pym}}\cdots\text{S}=\text{P}$ H-bonds, in **4** (H atoms not involved in H-bonding are omitted for clarity). Color code: C = black, H = light gray, N = blue, O = red, P = maroon, S = orange.

3 is the poorest one with respect to $\text{H}\cdots\text{H}$ components, which is explained by the presence of the CF_3 substituent. The shortest $\text{H}\cdots\text{H}$ distances are found in the corresponding 2D plots of the thioureas as distinctive spikes at $d_e + d_i \approx 2.2\text{--}2.6$ Å (Figures S2–S6 in the Supporting Information). Interestingly, a clear feature is seen in the 2D plots of **2–5**, where a division of the short $\text{H}\cdots\text{H}$ fingerprint is observed. This is due to the shortest interaction between three atoms.⁹² The intermolecular $\text{H}\cdots\text{H}$ contacts might result from dispersion dominated homopolar $\text{C}-\text{H}\cdots\text{C}-\text{H}$ interactions as it will be discussed in the forthcoming theoretical sections.

All the structures are also dictated by $\text{H}\cdots\text{S}$ contacts (19.1–23.8%) of the molecular surface (Table 5). These contacts are

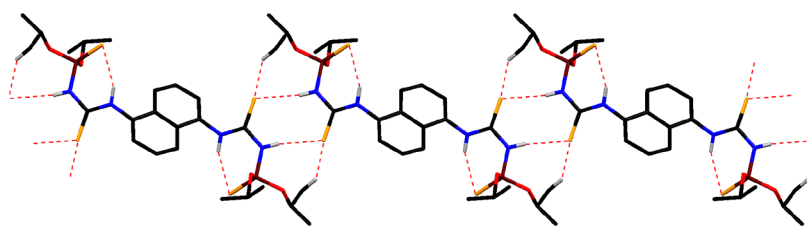


Figure 5. (P)N–H...S=C and C–H_{ipr}...S=C H-bonded 1D polymeric chain in **5** (H atoms not involved in H-bonding are omitted for clarity). Color code: C = black, H = light gray, N = blue, O = red, P = maroon, S = orange.

Table 2. Selected Bond Lengths (Å) and Angles (deg) for 1–5

	1	2	3	4	5
Bond lengths					
C=S	1.6753(19)	1.6856(19)	1.671(2)	1.660(2)	1.642(19)
P=S	1.9118(7)	1.9223(6)	1.9132(8)	1.9128(9)	1.906(8)
P–N	1.6711(17)	1.6681(17)	1.6787(19)	1.6771(19)	1.674(16)
C–N(C)	1.330(2)	1.324(2)	1.349(3)	1.374(3)	1.33(2)
C–N(P)	1.387(2)	1.391(2)	1.370(3)	1.352(3)	1.41(2)
Bond angles					
S=C–N(C)	125.88(14)	123.62(15)	123.30(16)	119.82(15)	125.8(14)
S=C–N(P)	118.81(13)	119.22(14)	120.10(15)	123.65(18)	119.0(14)
N–C–N	115.31(16)	117.16(16)	116.60(19)	119.5(2)	115.1(16)
P–N–C	130.74(12)	130.73(13)	131.88(15)	128.38(17)	125.4(13)
S=P–N	109.91(6)	111.73(6)	110.10(7)	118.17(7)	116.5(6)
Dihedral angles					
N–C–N–P	–10.2(3)	8.7(3)	–6.6(3)	176.78(14)	–29(2)
S=C–N–P	169.83(11)	–171.43(11)	173.62(12)	–2.1(3)	154.6(11)
S=P–N–C	179.68(15)	–179.89(14)	–172.81(16)	61.74(18)	56.3(16)
S=C–N–C	0.4(3)	0.2(3)	–1.0(3)	–179.37(16)	–6(3)

Table 3. Hydrogen Bond Lengths (Å) and Angles (deg) for 1–5

thiourea	D–H...A	<i>d</i> (D–H)	<i>d</i> (H...A)	<i>d</i> (D...A)	∠(DHA)
1^a	N(11)–H(11)...S(13) ^{#1}	0.86	2.53	3.3843(15)	171
	N(14)–H(14)...O(3)	0.86	2.57	3.122(2)	123
	N(14)–H(14)...O(7)	0.86	2.26	2.970(2)	140
	N(14)–H(14)...O(19)	0.86	2.33	2.689(3)	106
	N(14)–H(14)...O(19B)	0.86	2.27	2.640(7)	106
	O(19)–H(19)...O(3) ^{#2}	0.82	2.50	3.105(3)	132
2^b	N(11)–H(11)...S(13) ^{#1}	0.86	2.65	3.4052(16)	148
	N(14)–H(14)...O(3)	0.86	2.31	2.946(2)	131
	N(14)–H(14)...N(17)	0.86	2.46	2.816(2)	105
3^c	N(10)–H(10)...S(12) ^{#1}	0.88	2.44	3.2963(18)	165
	N(13)–H(13)...F(22)	0.88	2.47	2.861(3)	108
	N(13)–H(13)...O(3)	0.88	2.49	3.091(3)	126
	N(13)–H(13)...O(7)	0.88	2.48	3.058(2)	124
	C(4)–H(4)...S(2) ^{#2}	1.00	2.85	3.746(2)	150
	C(5)–H(5A)...F(23) ^{#3}	0.98	2.48	3.446(4)	170
4^d	N(11)–H(11)...N(16)	0.86	1.93	2.647(3)	140
	N(14)–H(14)...N(20) ^{#1}	0.86	2.23	3.084(3)	174
	C(18)–H(18)...S(2) ^{#2}	0.93	2.84	3.616(3)	142
	C(19)–H(19)...S(13) ^{#1}	0.93	2.78	3.576(3)	144
5^e	N(11)–H(11)...S(13) ^{#1}	0.88	2.62	3.370(17)	144
	N(14)–H(14)...S(1)	0.88	2.38	3.199(17)	155
	C(9)–H(9C)...S(13) ^{#1}	0.98	2.98	3.807	142

^aSymmetry transformations used to generate equivalent atoms: #1 1 – *x*, 2 – *y*, 2 – *z*; #2 – *x*, – *y*, 1 – *z*. ^bSymmetry transformations used to generate equivalent atoms: #1 2 – *x*, – *y*, 1 – *z*. ^cSymmetry transformations used to generate equivalent atoms: #1 1 – *x*, 1 – *y*, 2 – *z*; #2 – *x*, – *y*, 2 – *z*; #3 1 – *x*, – *y*, 2 – *z*. ^dSymmetry transformations used to generate equivalent atoms: #1 1 – *x*, 2 – *y*, 1 – *z*; #2 – 1 + *x*, *y*, *z*. ^eSymmetry transformations used to generate equivalent atoms: #1 1 – *x*, 1 – *y*, 1 – *z*.

found as a pair of sharp peaks at $d_e + d_i \approx 2.3$ – 2.7 Å (Figures S2–S6 in the Supporting Information) and attributed to

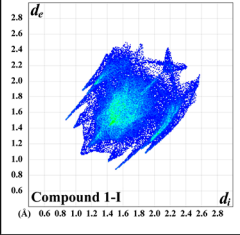
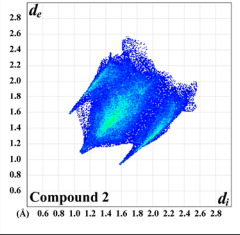
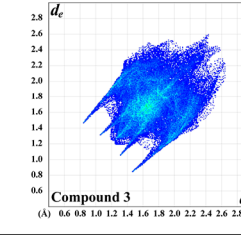
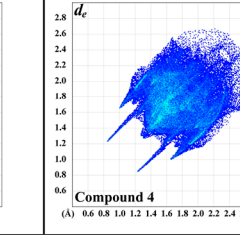
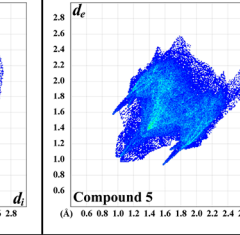
(P)N–H...S=C intermolecular H-bonds in **1**–**3** and **5**, and C–H_{pyr}...S=C and C–H_{pyr}...S=P hydrogen bonds in **4**

Table 4. $\pi\cdots\pi$ Interaction Distances (Å) and Angles (deg) for **3**^a

	Cg(I)	Cg(J)	$d[\text{Cg}(I)-\text{Cg}(J)]$	α	β	γ
3 ^b	Cg(C ₆ H ₄)	Cg(C ₆ H ₄) ^{#1}	3.8924(15)	0.00(12)	24.0	24.0

^aCg(I)–Cg(J): distance between ring centroids; α : dihedral angle between planes Cg(I) and Cg(J); β : angle Cg(I) → Cg(J) vector and normal to plane I; γ : angle Cg(I) → Cg(J) vector and normal to plane J. ^bSymmetry transformations used to generate equivalent atoms: #1 1 – x, – 1 – y, 1 – z.

Table 5. 2D Fingerprint Plots, Hirshfeld Contact Surfaces and Derived “Random Contacts” and “Enrichment Ratios” for **1–5**^a

	1-1					2					3					4					5					
																										
	(Å) 0.6 0.8 1.0 1.2 1.4 1.6 1.8 2.0 2.2 2.4 2.6 2.8					(Å) 0.6 0.8 1.0 1.2 1.4 1.6 1.8 2.0 2.2 2.4 2.6 2.8					(Å) 0.6 0.8 1.0 1.2 1.4 1.6 1.8 2.0 2.2 2.4 2.6 2.8					(Å) 0.6 0.8 1.0 1.2 1.4 1.6 1.8 2.0 2.2 2.4 2.6 2.8					(Å) 0.6 0.8 1.0 1.2 1.4 1.6 1.8 2.0 2.2 2.4 2.6 2.8					
	H	C	N	O	S	H	C	N	O	S	H	C	N	O	S	F	H	C	N	O	S	H	C	N	O	S
Contacts (C, %) ^b																										
H	71.3	–	–	–	–	69.6	–	–	–	–	44.0	–	–	–	–	51.1	–	–	–	–	54.0	–	–	–	–	
C	0.2	0.0	–	–	–	1.7	0.0	0.0	–	–	8.2	1.8	–	–	–	9.4	0.2	–	–	–	14.8	0.0	–	–	–	
N	0.0	0.0	0.0	–	–	1.4	0.0	0.0	–	–	0.7	0.0	0.0	–	–	10.2	0.0	0.1	–	–	2.0	0.0	0.0	–	–	
O	6.4	0.0	0.0	0.0	–	2.7	0.0	0.0	0.0	–	1.6	0.0	0.0	0.0	–	5.2	0.0	0.0	0.0	–	4.3	0.0	0.0	0.0	–	
S	20.3	0.0	0.0	0.3	1.4	23.8	0.0	0.0	0.0	0.7	21.6	0.0	0.0	0.0	0.8	19.1	1.9	2.8	0.0	0.0	22.4	1.0	0.4	1.1	0.0	
F	–	–	–	–	–	–	–	–	–	–	18.5	0.0	0.0	0.0	0.0	2.8	–	–	–	–	–	–	–	–	–	–
Surface (S, %)																										
	84.8	0.1	0.0	3.4	11.7	84.4	0.9	0.7	1.4	12.6	69.3	5.9	0.4	0.8	11.6	12.1	73.1	5.9	6.6	2.6	11.9	75.8	7.9	1.2	2.7	12.5
Random contacts (R, %)																										
H	71.9	–	–	–	–	71.2	–	–	–	–	48.0	–	–	–	–	53.4	–	–	–	–	57.5	–	–	–	–	
C	0.2	0.0	–	–	–	1.5	0.0	–	–	–	8.2	0.3	–	–	–	8.6	0.3	–	–	–	12.0	0.6	–	–	–	
N	0.0	0.0	0.0	–	–	1.2	0.0	0.0	–	–	0.6	0.0	0.0	–	–	9.6	0.8	0.4	–	–	1.8	0.2	0.0	–	–	
O	5.8	0.0	0.0	0.1	–	2.4	0.0	0.0	0.0	–	1.1	0.1	0.0	0.0	–	3.8	0.3	0.3	0.1	–	4.1	0.4	0.1	0.1	–	
S	19.8	0.0	0.0	0.8	1.4	21.3	0.2	0.2	0.4	1.6	16.1	1.4	0.1	0.2	1.3	17.4	1.4	1.6	0.6	1.4	19.0	2.0	0.3	0.7	1.6	
F	–	–	–	–	–	–	–	–	–	–	16.8	1.4	0.1	0.2	2.8	1.5	–	–	–	–	–	–	–	–	–	–
Enrichment (E) ^c																										
H	0.99	–	–	–	–	0.98	–	–	–	–	0.92	–	–	–	–	0.96	–	–	–	–	0.94	–	–	–	–	
C	–	–	–	–	–	1.13	–	–	–	–	1.00	–	–	–	–	1.09	–	–	–	–	1.23	–	–	–	–	
N	–	–	–	–	–	1.17	–	–	–	–	–	–	–	–	–	1.06	–	–	–	–	1.11	–	–	–	–	
O	1.10	–	–	–	–	1.13	–	–	–	–	1.45	–	–	–	–	1.37	–	–	–	–	1.05	–	–	–	–	
S	1.03	–	–	–	1.00	1.12	–	–	–	0.44	1.34	0.00	–	–	0.62	1.10	1.36	1.75	–	0.00	1.18	0.50	–	–	0.00	
F	–	–	–	–	–	–	–	–	–	–	1.10	0.00	–	–	0.00	1.87	–	–	–	–	–	–	–	–	–	–

^aNo contacts for the phosphorus atom were found, and, hence, it was not included under consideration. ^bValues are obtained from CrystalExplorer 3.1.⁹⁴ ^cThe enrichment ratios were not computed when the “random contacts” were lower than 0.9%, as they are not meaningful.⁹⁵

(Table 3). **3** is further characterized by a notable proportion of H \cdots F contacts (18.5%) (Table 5), which are also shown as a pair of sharp spikes at $d_e + d_i \approx 2.4$ Å (Figure S4 in the Supporting Information) due to C–H_{iPr} \cdots F–C hydrogen bonds (Table 3).

The next remarkable contributor into the molecular surface of **1–I** is H \cdots O interactions (6.4%) (Table 5) with the shortest contacts in the 2D plot shown as a pair of “horns” at $d_e + d_i \approx 2.4$ Å (Figure S2 in the Supporting Information). These are due to the O–H \cdots O–P intermolecular H-bonds (Table 3). A similar proportion of the same contacts was found in **4** and **5** (5.2 and 4.3%, respectively), while a significantly lesser amount is on the molecular surfaces of **2** and **3** (2.7 and 1.6%, respectively). The shortest H \cdots O was found on the 2D plots of **2–5** at $d_e + d_i \approx 2.7–3.1$ Å (Figure S2 in the Supporting Information).

1–I is additionally described by negligible proportions of S \cdots S, H \cdots C, and O \cdots S contacts (1.4, 0.2, and 0.3%, respectively). Negligible proportions of the former two (0.7 and 1.7%,

respectively) as well as H \cdots N contacts (1.4%) were also found on the molecular surface of **2**. The presence of the aryl rings in **3–5** increases a proportion of the H \cdots C (8.2, 9.4, and 14.8%, respectively). These contacts in 2D plots are observed as “wings” with the shortest $d_e + d_i \approx 2.8–3.0$ Å (Figures S4–S6 in the Supporting Information). They are typical for C–H \cdots π interactions.⁹² It is worth adding that the 2D plots of **3** and **4** each contain a number of points at large d_e and d_i (Table 4), which is similar to the 2D plots of benzene⁹² and phenyl-containing compounds,^{90,101,102} and characteristic to areas on the molecular surface without any close connections to nuclei in adjacent molecules.

The thiourea **4** is further dominated by H \cdots N contacts (10.2%) (Table 5) with the shortest ones shown as a pair of sharp spikes at $d_e + d_i \approx 2.1$ Å (Figure S5 in the Supporting Information) and are due to the (Pym)N–H \cdots N_{Pym} intermolecular H-bonds (Table 3). A negligible proportion of H \cdots N was found in **3** and **5** (0.7 and 2.0%, respectively).

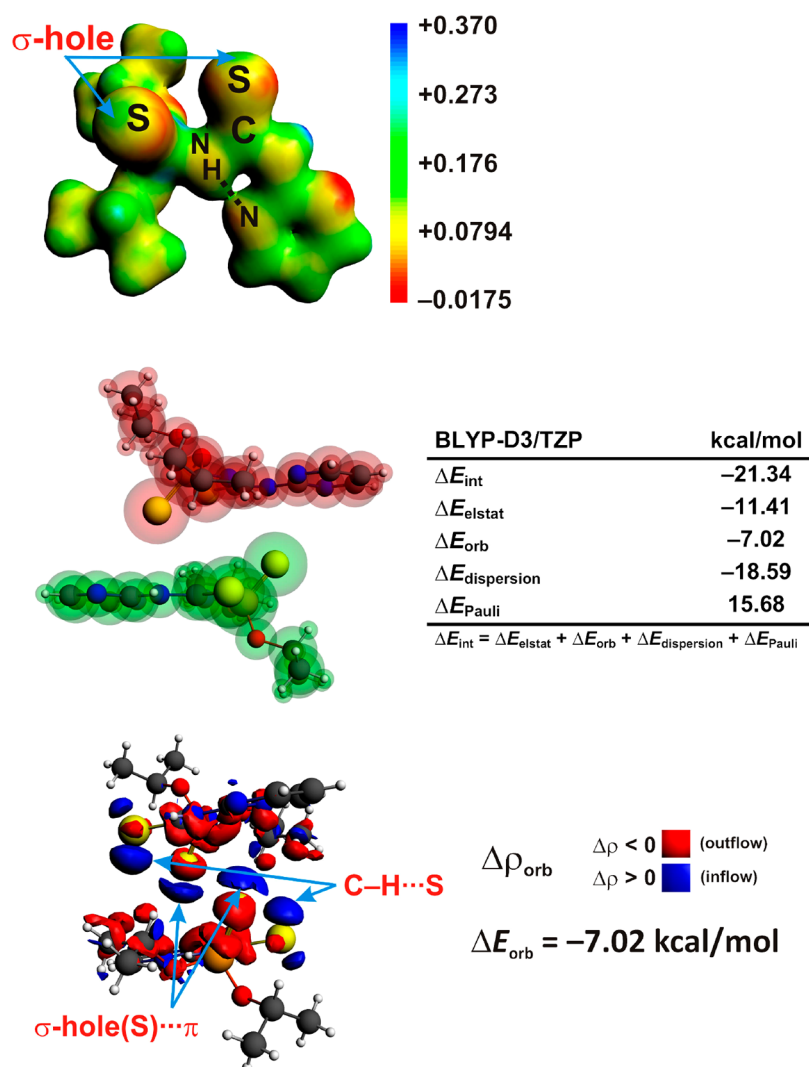


Figure 6. Molecular electrostatic potential for the monomer of **4** on the electron density isosurface 0.03 au (top), and fragmentation pattern (middle) and results of the ETS calculations (bottom) for the dimer of **4**.

The structure of **3** is also described by C...C and F...F contacts (1.8 and 2.8%, respectively). The former ones are found in the 2D plot as the area at $d_e = d_i \approx 1.8\text{--}2.0$ Å (Figure S4 in the Supporting Information) and characteristic to $\pi\cdots\pi$ stacking (Figure 3, Table 4). The F...F interactions are on the diagonal at $d_e = d_i \approx 1.6\text{--}2.0$ Å (Figure S4 in the Supporting Information) and responsible for the weak dihalogen bonding between the face-to-face oriented CF_3 groups of two adjacent molecules (Figure 3).¹⁰³

In order to examine the susceptibility of two species to be involved in a contact, we have calculated the enrichment ratios (E)⁹⁵ of the contacts for the studied thioureas. The H...H connections are enriched in all thioureas as evidenced from the enrichment ratios E_{HH} being close to unity (0.92–0.99) (Table 5). The E_{HO} and E_{HS} values are larger than unity (1.03–1.45), indicating that H...O and H...S have an increased propensity to form for all the structures. The E_{HC} values (1.00–1.23) confirm that these contacts also have a high propensity to form in **2–5** (Table 5). The H...N ($E_{\text{HN}} = 1.06\text{--}1.17$) contacts are highly favored in **2**, **4**, and **5**. Despite the negligible contribution of the S...S in **1-I** (1.4%), the corresponding proportion of R_{SS} is the same, yielding the enrichment ratio $E_{\text{SS}} = 1.00$. The same contacts are impoverished ($E_{\text{SS}} = 0.44\text{--}0.62$)

in **2** and **3**, which is explained by significantly higher values of the random contacts $R_{\text{SS}} = 1.3\text{--}1.6\%$ compared to proportions of these contacts (0.7–0.8%). A similar trend, but for the C...S, is observed in **4** and **5**. In particular, while **4** is highly enriched by C...S ($E_{\text{CS}} = 1.36$), the molecular surface of **5** is significantly impoverished ($E_{\text{CS}} = 0.50$). Finally, the N...S contacts are highly favored in **4** ($E_{\text{NS}} = 1.75$), while **3** is highly enriched by the H...F ($E_{\text{HF}} = 1.10$) and F...F ($E_{\text{FF}} = 1.87$) interactions.

At this stage we performed detailed qualitative and quantitative characterizations of various noncovalent interactions based on the charge and energy decomposition scheme ETS-NOCV⁹⁶ as available in the ADF package.^{104,105} Recently it was demonstrated that the BLYP-D3/TZP with the Slater basis sets performs well for weak interactions.^{106,107} To this end, we have applied herein this protocol. It also appeared to be reliable in our previous investigations.^{8,22,34}

We have determined, based on the molecular electrostatic potentials, that the NTTUs ($X = \text{S}$) monomers are characterized by the presence of decreased electron density at the tips of both sulfur atoms that indicates the so-called σ -holes^{39–43} (Figure 6). It is now well-known that it can lead to the formation of strong directional interactions with nucleophiles.^{39–43,108,109} Indeed, we have delineated herein

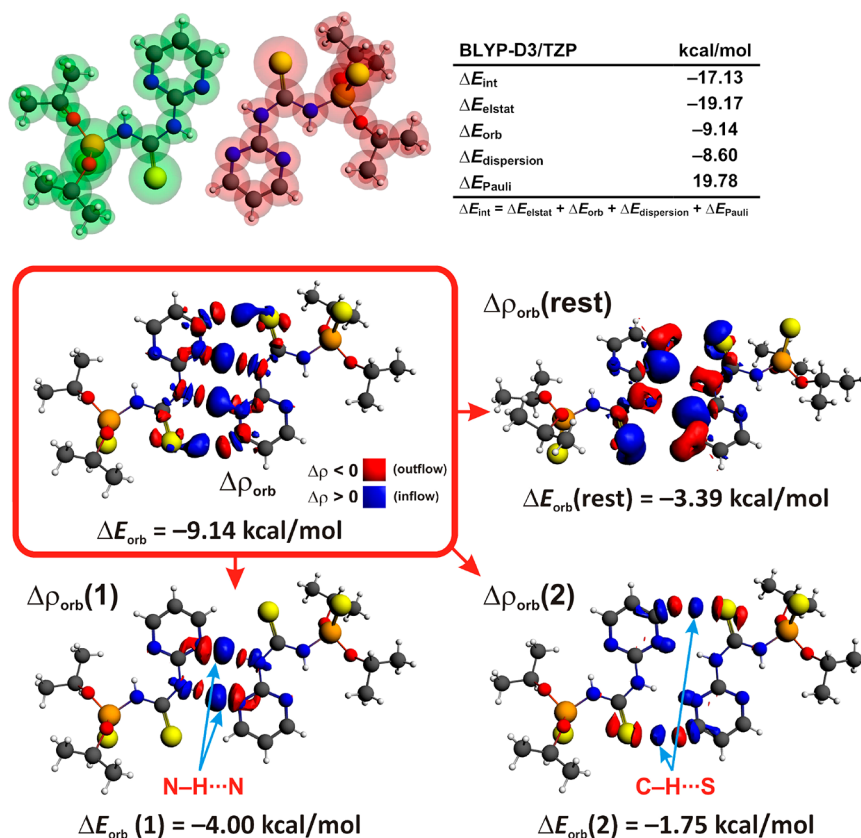


Figure 7. Dimeric model of **4** from the side-to-side interacting monomers and the ETS energy decomposition results (top) together with the NOCV-based deformation density contributions (bottom).

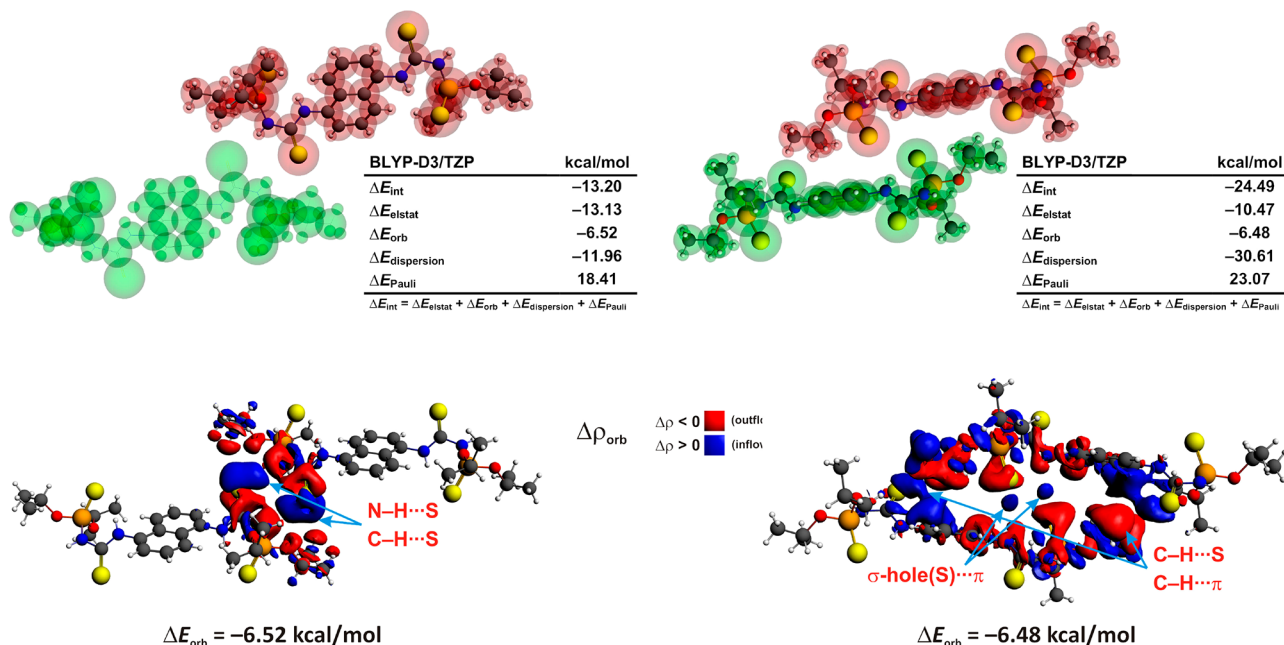


Figure 8. Dimeric models of **5** and the ETS energy decomposition results (top) together with the overall differential density quantities $\Delta \rho_{\text{orb}}$ and ΔE_{orb} (bottom).

due to the ETS-NOCV calculations that a dimer of **4**, containing parallel monomers, is extremely stable with the calculated interaction energy $\Delta E_{\text{int}} = -21.34$ kcal/mol (Figure 6). It stems mostly from the $\sigma\text{-hole(S)}\cdots\pi$ interaction formed between the thiophosphoryl sulfur $\sigma\text{-hole}$ and the (Pym)NH

π -system, which is further augmented by the presence of intermolecular $\text{C-H}_{\text{ipr}}\cdots\text{S}=\text{C}$ interactions. An inspection of the overall deformation density contour leads to the conclusion that the $\sigma\text{-hole(S)}\cdots\pi$ interaction is significantly covalent due to the charge delocalization from the $\pi(\text{HN}=\text{C})$ to the sulfur

tip area (Figure 6). Additionally, the electron depletion from the lone pair (Lp) of C=S into $\sigma^*(\text{C-H})$ is clearly seen due to the C-H_{ipr}...S=C interactions. The ETS-NOCV data testify that the London dispersion stabilization covers ~50% of the overall stabilization, followed by quite similarly important electrostatic (~31%) and charge delocalization (~19%) terms (Figure 6). We have additionally estimated the role of correlation energy in **4** (Figure 6) by performing HF and MP2 calculations, which was found to be -13.6 kcal/mol (Table S1 in the Supporting Information). This value is lower than the semiempirical D3 correction by ca. -21.34 kcal/mol. It is notable that at the HF level the overall interaction energy is only -4.2 kcal/mol (Table S1 in the Supporting Information). Other dispersion corrected XC and MP2 provide quite similar interaction energies to ADF/BLYP-D3/TZP (Table S1 in the Supporting Information). In the case of typical Lp... π interactions, the electrostatic stabilization were found to be a dominant factor followed by slightly less important dispersion energy and the least crucial charge delocalization term.¹¹⁰ Interestingly, when considering some anions, the charge delocalization contribution can be of vital importance as demonstrated by Kozelka and co-workers.^{111,112} It is important to highlight that such efficient stabilization obtained herein (Figure 6) is far stronger as compared to the known Lp... π interactions, which are typically within a few kcal/mol,¹¹⁰ and even the conventional hydrogen bonds.⁴⁴⁻⁴⁷

The interaction energy of monomers in **4**, interacting through the conventional ionic N-H...N H-bonds, is notably lower by ~4 kcal/mol compared to the dimer bounded through σ -hole(S)... π (Figures 6 and 7). It is important to comment that the major N-H...N stabilization is supported by weaker C-H...S interactions as indicated by the separated NOCV-deformation density channels $\Delta\rho_{\text{orb}}(1)$ and $\Delta\rho_{\text{orb}}(2)$ (Figure 7). The corresponding stabilizations are $\Delta E_{\text{orb}}(1) = -4.00$ kcal/mol and $\Delta E_{\text{orb}}(2) = -1.75$ kcal/mol (Figure 7). Interestingly, π -polarizations with $\Delta E_{\text{orb}}(\text{rest}) = -3.39$ kcal/mol are similar in strength to the leading N-H...N charge delocalization channel $\Delta E_{\text{orb}}(1) = -4.00$ kcal/mol (Figure 7).

In the case of **5** dispersion dominated σ -hole(S)... π interactions are even stronger than in **4**, $\Delta E_{\text{int}} = -24.49$ kcal/mol (Figure 8). This is due to the supportive C-H... π and C-H...S interactions (Figure 8). It is important to comment that instead of the typical N-H...N hydrogen bond the thioureas **1-3** and **5** contain N-H...S intermolecular interactions. ETS-NOCV allowed us to determine that N-H...S is also roughly two times weaker than σ -hole(S)... π and it is the strongest in **5** ($\Delta E_{\text{int}} = -13.20$ kcal/mol), whereas its strength is quite alike ($|\Delta E_{\text{int}}| \sim 9-10$ kcal/mol) in the remaining systems (Figures 8 and 9, and Figures S7-S9 in the Supporting Information). The London dispersion and electrostatic contributions are both leading stabilizing components and each cover ~40% of the overall stabilization of N-H...S followed by the charge delocalization term, ~20% (Figures 8 and 9, and Figures S7-S9 in the Supporting Information). It shall be referenced that in our previous investigations based on another set of R ligands lack of any σ -hole(S)... π interactions was noted, and the strongest N-H...S (supported by C-H...C-H, C-H...S and other contacts) constituted the crystals.⁹¹ We have further delineated qualitatively due to QTAIM and NCI calculations that C-H...C(π), σ -hole(S)...C(π), and C-H...C-H interactions can be quite similar in strength as opposed to notably stronger C-H...S (Figure S10 in the Supporting Information). It is important to highlight that apart

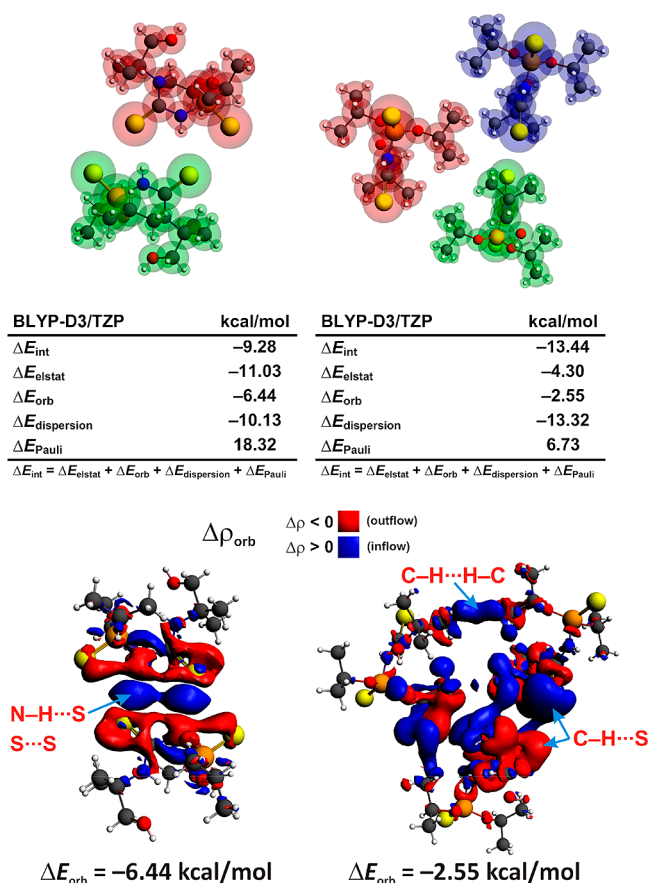


Figure 9. Dimeric and trimeric models of **1** and the ETS energy decomposition results (top) together with the overall differential density quantities $\Delta\rho_{\text{orb}}$ and ΔE_{orb} (bottom).

from the already discussed noncovalent interactions, **1** and **2** are further stabilized by nonconventional C-H...C-H and C-H...S contacts giving rise to dispersion dominated (~60%) trimeric interaction energies by $\Delta E_{\text{int}} = -13.44$ kcal/mol and -22.36 kcal/mol, respectively (Figure 9 and Figure S7 in the Supporting Information). Notably, the charge delocalization term is also non-negligible since it can cover ~15% of the overall stabilization (Figure 9 and Figure S7 in the Supporting Information). Although the typical face-to-face π ... π stacking, augmented by C-H...S contacts in the dimer of **3**, is the strongest, $\Delta E_{\text{int}} = -13.23$ kcal/mol, the slipped parallel model, which involves purely intermolecular homopolar C-H...C-H interactions between monomers, is only somewhat less stable, $\Delta E_{\text{int}} = -7.47$ kcal/mol (Figures S8 and S9 in the Supporting Information). Interestingly, the C-H...C-H engages interactions between the *i*Pr and aryl units, and quantitatively the charge delocalization contribution outweighs the electrostatic term with the obvious dominance of the London dispersion forces (Figure S9 in the Supporting Information). It is quantitatively and qualitatively comparable to the degree of joint C-H...F and C-H...S stabilization in **3** (Figures S8 and S9 in the Supporting Information).

CONCLUSIONS

In summary, we have synthesized a series of five novel thioureas RNHC(S)NHP(S)(O*i*Pr)₂ [R = (HOCH₂)(Me)₂C (**1**), Me₂CH₂CH₂ (**2**), 2-CF₃C₆H₄ (**3**), 2-Pym (**4**)] and bis-thiourea 1,5-C₁₀H₆{NHC(S)NHP(S)(O*i*Pr)₂} (**5**) by the

addition of thiophosphorylisothiocyanate to the corresponding amine. They were subsequently characterized by the NMR spectroscopy, X-ray diffraction, as well as theoretical ETS-NOCV charge and energy decomposition calculations. According to the NMR spectroscopy data of **5**, it was established that both amine groups of the 1,5-diaminonaphthalene reacted with the isothiocyanate. Furthermore, the NMR data testify that the thiourea **4** is completely in a zwitterionic form in CDCl_3 caused by strong intramolecular $\text{N}-\text{H}\cdots\text{N}$ interaction. Single crystal X-ray diffraction studies showed that an *E* arrangement of the $\text{C}=\text{S}$ and $\text{P}-\text{N}$ bonds in the $\text{S}=\text{C}-\text{N}-\text{P}$ backbones was found for all the thioureas except **4**, which exhibits a *Z* conformation of the same fragment. The $\text{S}=\text{P}-\text{N}-\text{C}$ backbone tends to be in an *E* conformation in the structures of **1-3**, and a *Z* conformation was observed in the structures of **4** and **5**.

We have determined that the monomers that constitute the obtained crystals are characterized by multiple conventional and nonconventional intramolecular noncovalent interactions including $\text{N}-\text{H}\cdots\text{X}$ ($\text{X} = \text{O}$, **1-3**; F , **3**; N , **4**; S , **5**) and $\text{C}-\text{H}\cdots\text{Y}$ ($\text{Y} = \text{O}$, **1**; N , **2** and **3**; S , **4** and **5**) augmented further by homopolar $\text{C}-\text{H}\cdots\text{H}-\text{C}$ contacts (**1-5**).

Hirshfeld surface analysis and associated 2D fingerprint plots, as well as the enrichment ratios, have shown that **1-5** are constituted mainly from $\text{H}\cdots\text{H}$ and $\text{H}\cdots\text{S}$ intermolecular contacts. This is mostly due to the numerous intermolecular homopolar $\text{C}-\text{H}\cdots\text{H}-\text{C}$ as well as $\text{X}-\text{H}\cdots\text{S}$ ($\text{X} = \text{C}$, N) interactions. The ETS charge and energy decomposition scheme allowed us to pinpoint the crucial role of London dispersion stabilization in both types of interactions. More specifically, in the case of intermolecular $\text{N}-\text{H}\cdots\text{S}$ interactions responsible for the formation of centrosymmetric $\text{R}_2^2(8)$ dimers or 1D polymeric chains, with the overall strength $|\Delta E_{\text{int}}|$ varying from ~ 9 kcal/mol up to 14 kcal/mol, London dispersion stabilization and electrostatic contributions are similarly crucial ($\sim 40\%$ of the overall stabilization) followed by the charge delocalization term (20%), whereas $\text{C}-\text{H}\cdots\text{H}-\text{C}$, $\text{C}-\text{H}\cdots\text{S}$, and $\text{C}-\text{H}\cdots\text{F}$ are dispersion dominated ($\sim 60\%$) with less efficient electrostatic ($\sim 25\%$) and charge delocalization contributions ($\sim 15\%$). It is clear that although $\text{C}-\text{H}\cdots\text{H}-\text{C}$, $\text{C}-\text{H}\cdots\text{S}$, and $\text{C}-\text{H}\cdots\text{F}$ engage in principle inert $\text{C}-\text{H}$ bonds, the charge outflow from the corresponding $\sigma(\text{C}-\text{H})$ bonds is discovered resulting in notable ΔE_{orb} values in the ETS-NOCV analyses—it is even superior over the electrostatic term in the case of slipped-parallel model of **3**. Finally, it is of great importance to stress that the already discovered intra- and intermolecular interactions are not the strongest ones. Surprisingly, we have delineated that the strongest are intermolecular $\sigma\text{-hole}(\text{S})\cdots\pi$ interactions noted in **4** and **5** with $|\Delta E_{\text{int}}| = 21.34$ and 24.49 kcal/mol, respectively. They are even stronger than typical ionic $\text{N}-\text{H}\cdots\text{N}$ bonds in **4** ($|\Delta E_{\text{int}}| = 17.13$ kcal/mol). As far as the nature of $\sigma\text{-hole}(\text{S})\cdots\pi$ is concerned, these noncovalent interactions determined herein are not, as other typical $\sigma\text{-hole}$ bonds, dominated by electrostatics.³⁹⁻⁴³ We have determined that again the London dispersion stabilization is a prevailing factor ($\sim 50\%$ of the overall stabilization), followed by quite similarly crucial electrostatic ($\sim 30\%$) and charge delocalization ($\sim 20\%$) components. The latter one stems from the charge depletion from the $\pi(\text{HN}=\text{C})$ and the accumulation at the tip of a sulfur region. Additionally, the electron depletion from the lone pair (Lp) of $\text{C}=\text{S}$ into $\sigma^*(\text{C}-\text{H})$ is clearly seen due to the supportive $\text{C}-\text{H}_{\text{lp}}\cdots\text{S}=\text{C}$ interactions. All discovered and

deeply studied intermolecular interactions constitute the 3D networks of the synthesized crystals.

We believe that this work, highlighting the crucial role of London dispersion forces as well as other non-negligible bonding contributions through the existence of multiple “old” and “novel” inter- and intramolecular interactions in sterically demanding NTTUs, will be also useful not only in crystal engineering but also in a number of other fields since large areas of polar and hydrophobic (dispersion donating) regions are certainly present in other systems.

■ ASSOCIATED CONTENT

Supporting Information

The Supporting Information is available free of charge on the ACS Publications website at DOI: 10.1021/acs.cgd.8b00783.

Description of geometrical parameters; contours of the reduced density gradient (NCI); 2D and decomposed 2D fingerprint plots of observed contacts; the results of NCI calculations; overall interaction energies (PDF)

Accession Codes

CCDC 1469627–1469631 contain the supplementary crystallographic data for this paper. These data can be obtained free of charge via www.ccdc.cam.ac.uk/data_request/cif, or by emailing data_request@ccdc.cam.ac.uk, or by contacting The Cambridge Crystallographic Data Centre, 12 Union Road, Cambridge CB2 1EZ, UK; fax: +44 1223 336033.

■ AUTHOR INFORMATION

Corresponding Authors

*E-mail: damir.a.safin@gmail.com, d.a.safin@utmn.ru (D.A.S.).

*E-mail: mitoraj@chemia.uj.edu.pl (M.P.M.).

ORCID

Mariusz P. Mitoraj: 0000-0001-5359-9107

Yann Garcia: 0000-0002-3105-0735

Damir A. Safin: 0000-0002-9080-7072

Notes

The authors declare no competing financial interest.

■ ACKNOWLEDGMENTS

This work was partially performed using the infrastructure and resources provided by the Research Resource Center “Natural Resource Management and Physico-Chemical Research”. DFT calculations were partially performed using the PL-Grid Infrastructure and resources provided by the ACC Cyfronet AGH (Cracow, Poland). M.P.M. acknowledges the financial support of the Polish National Science Center within the Sonata Bis Project 2017/26/E/ST4/00104. The Fonds National de la Recherche Scientifique-FNRS (PDR T.0102.15), WBI Poland, PAN-FNRS and COST action CM1305, supported this work.

■ REFERENCES

- (1) Wagner, J. P.; Schreiner, P. R. London dispersion in molecular chemistry-reconsidering steric effects. *Angew. Chem., Int. Ed.* **2015**, *54*, 12274.
- (2) Liptrot, D. J.; Power, P. P. London dispersion forces in sterically crowded inorganic and organometallic molecules. *Nature Rev. Chem.* **2017**, *1*, 0004.
- (3) Grimme, S.; Antony, J.; Ehrlich, S.; Krieg, H. A consistent and accurate ab initio parametrization of density functional dispersion

correction (DFT-D) for the 94 elements H-Pu. *J. Chem. Phys.* **2010**, *132*, 154104.

(4) Grimme, S.; Ehrlich, S.; Goerigk, L. Effect of the damping function in dispersion corrected density functional theory. *J. Comput. Chem.* **2011**, *32*, 1456.

(5) Jeziorski, B.; Moszynski, R.; Szalewicz, K. Perturbation Theory Approach to Intermolecular Potential Energy Surfaces of van der Waals Complexes. *Chem. Rev.* **1994**, *94*, 1887.

(6) Sokalski, W. A.; Roszak, S.; Hariharan, P. C.; Kaufman, J. J. Improved SCF interaction energy decomposition scheme corrected for basis set superposition effect. *Int. J. Quantum Chem.* **1983**, *23*, 847.

(7) Fokin, A.; Chernish, L. V.; Gunchenko, P. A.; Tikhonchuk, E. Y.; Hausmann, H.; Serafin, M.; Dahl, J. E. P.; Carlson, R. M. K.; Schreiner, P. R. Stable alkanes containing very long carbon-carbon bonds. *J. Am. Chem. Soc.* **2012**, *134*, 13641.

(8) Safin, D. A.; Babashkina, M. G.; Robeyns, K.; Mitoraj, M. P.; Kubisiak, P.; Garcia, Y. Influence of the Homopolar Dihydrogen Bonding C-H...H-C on Coordination Geometry: Experimental and Theoretical Studies. *Chem. - Eur. J.* **2015**, *21*, 16679.

(9) Wolters, L. P.; Koekkoek, R.; Bickelhaupt, F. M. Role of Steric Attraction and Bite-Angle Flexibility in Metal-Mediated C-H Bond Activation. *ACS Catal.* **2015**, *5*, 5766.

(10) Mandal, N.; Pratik, S. M.; Datta, A. Exploring Ultrashort Hydrogen-Hydrogen Nonbonded Contacts in Constrained Molecular Cavities. *J. Phys. Chem. B* **2017**, *121*, 825.

(11) Firouzi, R.; Shahbazian, S. Seeking Extremes in Molecular Design: To What Extent May Two "Non-Bonded" Hydrogen Atoms be Squeezed in a Hydrocarbon? *ChemPhysChem* **2016**, *17*, 51.

(12) Rösel, S.; Quanz, H.; Logemann, C.; Becker, J.; Mossou, E.; Cañadillas-Delgado, L.; Caldeyher, E.; Grimme, S.; Schreiner, P. R. London Dispersion Enables the Shortest Intermolecular Hydrocarbon H...H Contact. *J. Am. Chem. Soc.* **2017**, *139*, 7428.

(13) de Almeida, L. R.; Carvalho, P. S., Jr; Napolitano, H. B.; Oliveira, S. S.; Camargo, A. J.; Figueredo, A. S.; de Aquino, G. L. B.; Carvalho-Silva, V. H. Contribution of Directional Dihydrogen Interactions in the Supramolecular Assembly of Single Crystals: Quantum Chemical and Structural Investigation of C₁₇H₁₇N₃O₂ Azine. *Cryst. Growth Des.* **2017**, *17*, 5145.

(14) Matta, C. F.; Hernández-Trujillo, J.; Tang, T. H.; Bader, R. F. W. Hydrogen-hydrogen bonding: a stabilizing interaction in molecules and crystals. *Chem. - Eur. J.* **2003**, *9*, 1940.

(15) Poater, J.; Solà, M.; Bickelhaupt, F. M. Hydrogen-Hydrogen Bonding in Planar Biphenyl, Predicted by Atoms-In-Molecules Theory, Does Not Exist. *Chem. - Eur. J.* **2006**, *12*, 2889.

(16) Bader, R. F. W. Pauli Repulsions Exist Only in the Eye of the Beholder. *Chem. - Eur. J.* **2006**, *12*, 2896.

(17) Pendás, A. M.; Francisco, E.; Blanco, M. A.; Gatti, C. Bond paths as privileged exchange channels. *Chem. - Eur. J.* **2007**, *13*, 9362.

(18) Eskandari, K.; Van Alsenoy, C. Hydrogen-hydrogen interaction in planar biphenyl: a theoretical study based on the interacting quantum atoms and Hirshfeld atomic energy partitioning methods. *J. Comput. Chem.* **2014**, *35*, 1883.

(19) Cukrowski, I. IQA-embedded fragment attributed molecular system energy change in exploring intramolecular interactions. *Comput. Theor. Chem.* **2015**, *1066*, 62.

(20) Weinhold, F.; Schleyer, P. R.; McKee, W. C. Bay-type H...H "bonding" in cis-2-butene and related species: QTAIM versus NBO description. *J. Comput. Chem.* **2014**, *35*, 1499.

(21) Matta, C. F.; Sadjadi, S. A.; Braden, D. A.; Frenking, G. The barrier to the methyl rotation in Cis-2-butene and its isomerization energy to Trans-2-butene, revisited. *J. Comput. Chem.* **2016**, *37*, 143.

(22) Cukrowski, I.; Sagan, F.; Mitoraj, M. P. On the Stability of Cis- and Trans-2-Butene Isomers. An Insight Based on the FAMSEC, IQA, and ETS-NOCV Schemes. *J. Comput. Chem.* **2016**, *37*, 2783.

(23) Ravindran, P.; Vajeeston, P.; Vidya, R.; Kjekshus, A.; Fjellvåg, H. Violation of the Minimum HH Separation "Rule" for Metal Hydrides. *Phys. Rev. Lett.* **2002**, *89*, 106403.

(24) Schouwink, P.; Hagemann, H.; Embs, J. P.; D'Anna, V.; Černý, R. Di-hydrogen contact induced lattice instabilities and structural

dynamics in complex hydride perovskites. *J. Phys.: Condens. Matter* **2015**, *27*, 265403.

(25) Wolstenholme, D. J.; Dobson, J. L.; McGrady, G. S. Homopolar dihydrogen bonding in main group hydrides: discovery, consequences, and applications. *Dalton Trans.* **2015**, *44*, 9718 and references therein..

(26) Sagan, F.; Filas, R.; Mitoraj, M. P. Non-Covalent Interactions in Hydrogen Storage Materials LiN(CH₃)₂BH₃ and KN(CH₃)₂BH₃. *Crystals* **2016**, *6*, 28.

(27) Echeverría, J.; Aullón, G.; Alvarez, S. Dihydrogen intermolecular contacts in group 13 compounds: H...H or E...H (E = B, Al, Ga) interactions? *Dalton Trans.* **2017**, *46*, 2844.

(28) Yourdkhani, S.; Jabłoński, M.; Echeverría, J. Attractive PH...HP interactions revealed by state-of-the-art ab initio calculations. *Phys. Chem. Chem. Phys.* **2017**, *19*, 28044.

(29) Echeverría, J. Abundance and Strength of M-H...H-C (M = Al, Ga, In) Dihydrogen Bonds. *Cryst. Growth Des.* **2017**, *17*, 2097.

(30) Echeverría, J.; Aullón, G.; Alvarez, S. Intermolecular interactions in group 14 hydrides: Beyond C-H...H-C contacts. *Int. J. Quantum Chem.* **2017**, *117*, e25432.

(31) Custelcean, R.; Jackson, J. E. Dihydrogen bonding: structures, energetics, and dynamics. *Chem. Rev.* **2001**, *101*, 1963.

(32) Mitoraj, M. P. Bonding in Ammonia Borane: An Analysis Based on the Natural Orbitals for Chemical Valence and the Extended Transition State Method (ETS-NOCV). *J. Phys. Chem. A* **2011**, *115*, 14708.

(33) Chen, X.; Zhao, J. C.; Shore, S. G. The roles of dihydrogen bonds in amine borane chemistry. *Acc. Chem. Res.* **2013**, *46*, 2666.

(34) Sagan, F.; Piękoś, Ł.; Andrzejak, M.; Mitoraj, M. P. From Saturated BN Compounds to Isoelectronic BN/CC Counterparts: An Insight from Computational Perspective. *Chem. - Eur. J.* **2015**, *21*, 15299.

(35) Belkova, N. V.; Epstein, L. M.; Filippov, O. A.; Shubina, E. S. Hydrogen and Dihydrogen Bonds in the Reactions of Metal Hydrides. *Chem. Rev.* **2016**, *116*, 8545.

(36) Gamez, P.; Mooibroek, T. J.; Teat, S. J.; Reedijk, J. Anion Binding Involving π -Acidic Heteroaromatic Rings. *Acc. Chem. Res.* **2007**, *40*, 435.

(37) Frontera, A.; Gamez, P.; Mascal, M.; Mooibroek, T. J.; Reedijk, J. Putting anion- π interactions into perspective. *Angew. Chem., Int. Ed.* **2011**, *50*, 9564.

(38) Safin, D. A.; Pialat, A.; Leitch, A. A.; Tumanov, N. A.; Korobkov, I.; Filinchuk, Y.; Brusso, J. L.; Murugesu, M. Anion-induced AgI self-assemblies with electron deficient aromatic ligands: anion- π -system interactions as a driving force for templated coordination networks. *Chem. Commun.* **2015**, *51*, 9547.

(39) Politzer, P.; Murray, J. S.; Clark, T. Halogen bonding: an electrostatically-driven highly directional noncovalent interaction. *Phys. Chem. Chem. Phys.* **2010**, *12*, 7748.

(40) Scheiner, S. The Pnictogen Bond: Its Relation to Hydrogen, Halogen, and Other Noncovalent Bonds. *Acc. Chem. Res.* **2013**, *46*, 280.

(41) Bauzá, A.; Mooibroek, T.; Frontera, A. Tetrel Bonding Interactions. *Chem. Rec.* **2016**, *16*, 473.

(42) Grabowski, S. J.; Sokalski, W. A. Are Various σ -Hole Bonds Steered by the Same Mechanisms? *ChemPhysChem* **2017**, *18*, 1569.

(43) Gleiter, R.; Haberhauer, G.; Werz, D. B.; Rominger, F.; Bleiholder, C. From Noncovalent Chalcogen-Chalcogen Interactions to Supramolecular Aggregates: Experiments and Calculations. *Chem. Rev.* **2018**, *118*, 2010.

(44) Lehn, J. M. *Supramolecular Chemistry*; VCH, Weinheim, Germany, 1995.

(45) Jeffery, G. A. *An Introduction To Hydrogen Bonding*; Oxford University Press, 1997.

(46) Moulton, B.; Zaworotko, M. J. From molecules to crystal engineering: supramolecular isomerism and polymorphism in network solids. *Chem. Rev.* **2001**, *101*, 1629.

(47) Grabowski, S. What Is the Covalency of Hydrogen Bonding? *Chem. Rev.* **2011**, *111*, 2597 and references therein..

- (48) Hollingsworth, M. D.; Harris, K. D. M. *Urea, Thiourea and Selenourea*, in *Comprehensive Supramolecular Chemistry*, ed. Atwood, J. L.; Davis, J. E. D.; MacNicol, D. D.; Vögtle, F. Pergamon, Oxford, UK, 1996; p 177.
- (49) Schmidtchen, F. P.; Berger, M. *Artificial Organic Host Molecules for Anions*. *Chem. Rev.* **1997**, *97*, 1609.
- (50) Harris, K. D. M. Meldola Lecture: understanding the properties of urea and thiourea inclusion compounds. *Chem. Soc. Rev.* **1997**, *26*, 279.
- (51) Beer, P. D.; Gale, P. A. Anion Recognition and Sensing: The State of the Art and Future Perspectives. *Angew. Chem., Int. Ed.* **2001**, *40*, 486.
- (52) Choi, K. H.; Hamilton, A. D. Macrocyclic anion receptors based on directed hydrogen bonding interactions. *Coord. Chem. Rev.* **2003**, *240*, 101.
- (53) Custelcean, R. Crystal engineering with urea and thiourea hydrogen-bonding groups. *Chem. Commun.* **2008**, 295.
- (54) Steed, J. W. Anion-tuned supramolecular gels: a natural evolution from urea supramolecular chemistry. *Chem. Soc. Rev.* **2010**, *39*, 3686.
- (55) Hay, B. P. De novo structure-based design of anion receptors. *Chem. Soc. Rev.* **2010**, *39*, 3700.
- (56) Li, A.-F.; Wang, J.-H.; Wang, F.; Jiang, Y.-B. Anion complexation and sensing using modified urea and thiourea-based receptors. *Chem. Soc. Rev.* **2010**, *39*, 3729.
- (57) Gale, P. A. Anion receptor chemistry: highlights from 2008 and 2009. *Chem. Soc. Rev.* **2010**, *39*, 3746.
- (58) Amendola, V.; Fabbri, L.; Mosca, L. Anion recognition by hydrogen bonding: urea-based receptors. *Chem. Soc. Rev.* **2010**, *39*, 3889.
- (59) Dydio, P.; Lichosyt, D.; Jurczak, J. Amide- and urea-functionalized pyrroles and benzopyrroles as synthetic, neutral anion receptors. *Chem. Soc. Rev.* **2011**, *40*, 2971.
- (60) Sokolov, F. D.; Safin, D. A.; Zabirow, N. G.; Verat, A. Y.; Brusko, V. V.; Krivolapov, D. B.; Mironova, E. V.; Litvinov, I. A. Synthesis, structure and properties of novel N-thiophosphorylated derivatives of 1,3-dihydro-2H-benzimidazol-2-imine and imidazolidine-2-imine. *Polyhedron* **2006**, *25*, 3611.
- (61) Safin, D. A.; Babashkina, M. G.; Sokolov, F. D.; Zabirow, N. G.; Galezowska, J.; Kozłowski, H. Complexes of a novel N-(diisopropylthiophosphoryl)thiourea derivative of 1,4,8,11-tetraazacyclotetradecane with Na⁺, K⁺ and Cu(PPh₃)²⁺ cations. *Polyhedron* **2007**, *26*, 1113.
- (62) Sokolov, F. D.; Safin, D. A.; Babashkina, M. G.; Zabirow, N. G.; Brusko, V. V.; Mironov, N. A.; Krivolapov, D. B.; Litvinov, I. A.; Cherkasov, R. A.; Solomonov, B. N. A "sodium trap" based on benzo-15-crown-5 with an exocyclic N-(thiophosphoryl)thiourea moiety. *Polyhedron* **2007**, *26*, 1550.
- (63) Safin, D. A.; Sokolov, F. D.; Szyrwił, Ł.; Babashkina, M. G.; Gimadiev, T. R.; Hahn, F. E.; Kozłowski, H.; Krivolapov, D. B.; Litvinov, I. A. Nickel(II) complexes with N-(thio)phosphorylthioureas AdNHC(S)NHP(X)(OiPr)₂: Versatile coordination of phosphoryl (X = O) and thiophosphoryl (X = S) derivatives. *Polyhedron* **2008**, *27*, 2271.
- (64) Sokolov, F. D.; Safin, D. A.; Bolte, M.; Shkairova, E. R.; Babashkina, M. G. New bifunctional N-thiophosphorylated thiourea and 2,5-dithiobiurea derivatives. Crystal structures of R[C(S)NHP(S)(OiPr)₂]₂ (R = -N(Ph)CH₂CH₂N(Ph)- and -NHNH-). *Polyhedron* **2008**, *27*, 3141.
- (65) Safin, D. A.; Sokolov, F. D.; Gimadiev, T. R.; Brusko, V. V.; Babashkina, M. G.; Chubukaeva, D. R.; Krivolapov, D. B.; Litvinov, I. A. Complexes of N-Thiophosphorylthiourea tBuNHC(S)NHP(S)(OiPr)₂ with Zinc(II), Cadmium(II), Nickel(II), and Cobalt(II) Cations. *Z. Anorg. Allg. Chem.* **2008**, *634*, 967.
- (66) Babashkina, M. G.; Safin, D. A.; Szyrwił, Ł.; Kubiak, M.; Sokolov, F. D.; Starikov, Y. V.; Kozłowski, H. Complexes of N-Thiophosphorylthiourea α-NaphthylNHC(S)NHP(S)(OiPr)₂ (HL) with Copper(I). Crystal Structures of HL and Cu(PPh₃)₂L. *Z. Anorg. Allg. Chem.* **2009**, *635*, 554.
- (67) Babashkina, M. G.; Safin, D. A.; Bolte, M.; Klein, A. Intramolecular hydrogen bond controlled coordination of N-thiophosphorylated thiourea 2,6-Me₂C₆H₃NHC(S)NHP(S)(OiPr)₂ with Ni(II). *Inorg. Chem. Commun.* **2009**, *12*, 678.
- (68) Safin, D. A.; Bolte, M.; Shkairova, E. R.; Babashkina, M. G. The influence of the substituent [PhNHNH- and EtN(NH₂)-] on the N-thiophosphorylated thiosemicarbazides RC(S)NHP(S)(OiPr)₂ crystal design. *Polyhedron* **2009**, *28*, 501.
- (69) Safin, D. A.; Babashkina, M. G.; Bolte, M.; Klein, A. The influence of the spacer Z on N-phosphorylated bis-thioureas and 2,5-dithiobiurea Z[C(S)NHP(O)(OiPr)₂]₂ (Z = NHCH₂CH₂NH, NHC₆H₄-2-NH, NHNH) crystal design. *Polyhedron* **2009**, *28*, 1403.
- (70) Babashkina, M. G.; Safin, D. A.; Bolte, M.; Klein, A. Synthesis of N-(thio)phosphorylated thiosemicarbazides RC(S)NHP(X)(OiPr)₂ (X = S, R = NH₂N(Me)-; X = O, R = NH₂N(Me)-, PhNHNH-): Reaction of NH₂N(Me)C(S)NHP(S)(OiPr)₂ with acetone. *Polyhedron* **2009**, *28*, 2693.
- (71) Luckay, R. C.; Sheng, X.; Strasser, C. E.; Raubenheimer, H. G.; Safin, D. A.; Babashkina, M. G.; Klein, A. Competitive bulk liquid membrane transport and solvent extraction of some metal ions using RC(S)NHP(X)(OiPr)₂ (X = O, S) as ionophores. Formation of the polynuclear complex of [Ag(N≡C-NP(S)(OiPr)₂]_n. *Dalton Trans.* **2009**, 8227.
- (72) Safin, D. A.; Babashkina, M. G.; Klein, A. Copper(I) Complexes of N-thiophosphorylated Bis-thiourea [CH₂NHC(S)NHP(S)(OiPr)₂]₂ and Phosphines (PPh₃, Ph₂P(CH₂)₁₋₃PPh₂, Ph₂P(C₅H₄FeC₅H₄)PPh₂): Versatile Structures and Luminescence. *Croat. Chem. Acta* **2010**, *83*, 353.
- (73) Safin, D. A.; Babashkina, M. G.; Bolte, M.; Klein, A. Tetraphenylphosphonium salts of N-thiophosphorylated thiobenzamide, mono-thioureas or bis-thioureas. *Heteroat. Chem.* **2010**, *21*, 343.
- (74) Babashkina, M. G.; Safin, D. A. Complexes of [(iPrO)₂P(O)NHC(S)NHCH₂]₂CH₂ with Co(II), Ni(II), Zn(II), and Pd(II): Reaction of [(iPrO)₂P(O)NHC(S)NHCH₂]₂ with KOH Leading to the Imidazolidine-2-Imine Derivative. *Phosphorus, Sulfur Silicon Relat. Elem.* **2010**, *185*, 1437.
- (75) Babashkina, M. G.; Shkairova, E. R.; Safin, D. A.; Sokolov, F. D.; Klein, A.; Szyrwił, Ł.; Kubiak, M.; Kozłowski, H.; Krivolapov, D. B. Dinuclear Complexes of Copper(I) with Crown Ether-containing N-Thiophosphorylated Bis-thioureas and 2,2'-Bipyridine or 1,10-Phenanthroline: Synthesis, Characterization, and Picrate Extraction Properties. *Z. Anorg. Allg. Chem.* **2010**, *636*, 2626.
- (76) Babashkina, M. G.; Safin, D. A.; Klein, A.; Bolte, M. Synthesis, Characterisation and Luminescent Properties of Mixed-Ligand Copper(I) Complexes Incorporating N-Thiophosphorylated Thioureas and Phosphane Ligands. *Eur. J. Inorg. Chem.* **2010**, *2010*, 4018.
- (77) Safin, D. A.; Babashkina, M. G.; Bolte, M.; Klein, A. Synthesis, characterization and complexation properties of N-phosphorylated thioureas RNHC(S)NHP(O)(OiPr)₂ (R = 2-Py, 3-Py) towards Ni(II). *Inorg. Chim. Acta* **2010**, *363*, 1791.
- (78) Safin, D. A.; Babashkina, M. G.; Bolte, M.; Köckerling, M. Heteroligand copper(I) complexes of N-thiophosphorylated thioureas and phosphanes: Versatile structures and luminescence. *Inorg. Chim. Acta* **2011**, *370*, 59.
- (79) Babashkina, M. G.; Safin, D. A.; Bolte, M.; Srebro, M.; Mitoraj, M.; Uthe, A.; Klein, A.; Köckerling, M. Intramolecular hydrogen bonding controls 1,3-N,S- vs. 1,5-S,S'-coordination in Ni^{II} complexes of N-thiophosphorylated thioureas RNHC(S)NHP(S)(OiPr)₂. *Dalton Trans.* **2011**, *40*, 3142.
- (80) Babashkina, M. G.; Safin, D. A.; Srebro, M.; Kubisiak, P.; Mitoraj, M. P.; Bolte, M.; Garcia, Y. Solvent-induced 1,3-N,S- vs. 1,5-S,S'-coordination in the Ni^{II} complex [Ni{p-Me₂NC₆H₄NHC(S)NP(S)(OiPr)₂]₂. *CrystEngComm* **2011**, *13*, 5321.
- (81) Babashkina, M. G.; Safin, D. A.; Robeyns, K.; Brzuszkiewicz, A.; Kozłowski, H.; Garcia, Y. Thiophosphorylated bis-thioureas for competitive bulk liquid membrane transport of some metal ions. *CrystEngComm* **2012**, *14*, 1324.

- (82) Babashkina, M. G.; Safin, D. A.; Garcia, Y. Heteroleptic Cu(I) and Ag(I) complexes of N-thiophosphorylated tris-thioureas and triphenylphosphane. *Polyhedron* **2012**, *33*, 114.
- (83) Babashkina, M. G.; Safin, D. A.; Robeyns, K.; Garcia, Y. Complexation properties of the crown ether-containing N-thiophosphorylated thiourea towards Ni(II). *Dalton Trans.* **2012**, *41*, 1451.
- (84) Babashkina, M. G.; Safin, D. A.; Bolte, M.; Garcia, Y. N-(Diisopropylthiophosphoryl)-N'-(R)-thioureas: synthesis, characterization, crystal structures and competitive bulk liquid membrane transport of some metal ions. *Dalton Trans.* **2012**, *41*, 3223.
- (85) Safin, D. A.; Babashkina, M. G.; Railliet, A. P.; Tumanov, N. A.; Robeyns, K.; Devlin, E.; Sanakis, Y.; Filinchuk, Y.; Garcia, Y. First structurally characterized self-assembly of bipodal N-thiophosphorylated bis-thiourea with Co(II): magnetic properties and thermal decomposition. *Dalton Trans.* **2013**, *42*, 5532.
- (86) Safin, D. A.; Babashkina, M. G.; Robeyns, K.; Mitoraj, M. P.; Kubisiak, P.; Brela, M.; Garcia, Y. Experimental and theoretical investigations of the Ni^{II} complex with N-phosphorylated thiourea *iPrNHC(S)NHP(O)(OPh)₂*. *CrystEngComm* **2013**, *15*, 7845.
- (87) Safin, D. A.; Babashkina, M. G.; Bolte, M.; Garcia, Y. Tetranuclear assembly of palladium(II): Catalyst for C–C coupling reactions. *Polyhedron* **2013**, *62*, 133.
- (88) Safin, D. A.; Babashkina, M. G.; Robeyns, K.; Bolte, M.; Garcia, Y. N-Salicylidene aniline derivatives based on the N'-thiophosphorylated thiourea scaffold. *CrystEngComm* **2014**, *16*, 7053.
- (89) Babashkina, M. G.; Safin, D. A.; Robeyns, K.; Garcia, Y. A Neutral 1D Coordination Polymer Constructed from the Ni^{II} Complex of the N-Phosphorylated Thiourea PhNHC(S)NHP(O)(OPh)₂ and Pyrazine: A Single-Source Precursor for Nickel Nanoparticles. *Eur. J. Inorg. Chem.* **2015**, *2015*, 1160.
- (90) Babashkina, M. G.; Robeyns, K.; Filinchuk, Y.; Safin, D. A. Detailed studies of the interaction of 3-chloroaniline with O,O'-diphenylphosphorylthiocyanate. *New J. Chem.* **2016**, *40*, 1230.
- (91) Mitoraj, M. P.; Sagan, F.; Babashkina, M. G.; Isaev, A. Y.; Chichigina, Y. M.; Safin, D. A. N-Thiophosphorylthioureas RNHC(S)NHP(S)(OiPr)₂ as an Excellent Platform for Studying Synergy Between Hydrogen-Hydrogen Bonding and Other Families of Non-Covalent Interactions. *Eur. J. Org. Chem.* **2018**, submitted.
- (92) Spackman, M. A.; McKinnon, J. J. Fingerprinting intermolecular interactions in molecular crystal. *CrystEngComm* **2002**, *4*, 378.
- (93) Spackman, M. A.; Jayatilaka, D. Hirshfeld surface analysis. *CrystEngComm* **2009**, *11*, 19.
- (94) Wolff, S. K.; Grimwood, D. J.; McKinnon, J. J.; Turner, M. J.; Jayatilaka, D.; Spackman, M. A. *CrystalExplorer 3.1*; University of Western: Australia, 2012.
- (95) Jelsch, C.; Ejsmont, K.; Huder, L. The enrichment ratio of atomic contacts in crystals, an indicator derived from the Hirshfeld surface analysis. *IUCr* **2014**, *1*, 119.
- (96) Mitoraj, M. P.; Michalak, A.; Ziegler, T. A Combined Charge and Energy Decomposition Scheme for Bond Analysis. *J. Chem. Theory Comput.* **2009**, *5*, 962.
- (97) Rigaku Oxford Diffraction, CrysAlis(Pro) Software system, version 1.171.36.21, Rigaku Corporation, Oxford, UK, 2012.
- (98) Sheldrick, G. M. Crystal structure refinement with SHELXL. *Acta Crystallogr., Sect. A: Found. Crystallogr.* **2008**, *64*, 112.
- (99) Bruno, I. J.; Cole, J. C.; Edgington, P. R.; Kessler, M.; Macrae, C. F.; McCabe, P.; Pearson, J.; Taylor, R. New software for searching the Cambridge Structural Database and visualizing crystal structures. *Acta Crystallogr., Sect. B: Struct. Sci.* **2002**, *58*, 389.
- (100) Sokolov, F. D.; Brusko, V. V.; Zabirow, N. G.; Cherkasov, R. A. N-Acylamidophosphinates: Structure, Properties and Complexation Towards Main Group Metal Cations. *Curr. Org. Chem.* **2006**, *10*, 27.
- (101) Safin, D. A.; Mitoraj, M. P.; Robeyns, K.; Filinchuk, Y.; Velde, C. M. L. Luminescent mononuclear mixed ligand complexes of copper(I) with 5-phenyl-2,2'-bipyridine and triphenylphosphine. *Dalton Trans.* **2015**, *44*, 16824.
- (102) Safin, D. A.; Robeyns, K.; Babashkina, M. G.; Filinchuk, Y.; Rotaru, A.; Jureschi, C.; Mitoraj, M. P.; Hooper, J.; Brela, M.; Garcia, Y. Polymorphism driven optical properties of an anil dye. *CrystEngComm* **2016**, *18*, 7249.
- (103) Desiraju, G. R.; Parthasarathy, R. The nature of halogen-cntdot.cntdot.cntdot.halogen interactions: are short halogen contacts due to specific attractive forces or due to close packing of nonspherical atoms? *J. Am. Chem. Soc.* **1989**, *111*, 8725.
- (104) Te Velde, G.; Bickelhaupt, F. M.; Baerends, E. J.; Fonseca Guerra, C.; van Gisbergen, S. J. A.; Snijders, J. G.; Ziegler, T. Chemistry with ADF. *J. Comput. Chem.* **2001**, *22*, 931 and references therein.
- (105) Baerends, E. J.; Ziegler, T.; Autschbach, J.; Bashford, D.; Bérces, A.; Bickelhaupt, F. M.; Bo, C.; Boerrigter, P. M.; Cavallo, L.; Chong, D. P.; Deng, L.; Dickson, R. M.; Ellis, D. E.; van Faassen, M.; Fan, L.; Fischer, T. H.; Fonseca Guerra, C.; Franchini, M.; Ghysels, A.; Giammona, A.; van Gisbergen, S. J. A.; Götz, A. W.; Groeneveld, J. A.; Gritsenko, O. V.; Grüning, M.; Gusarov, S.; Harris, F. E.; van den Hoek, P.; Jacob, C. R.; Jacobsen, H.; Jensen, L.; Kaminski, J. W.; van Kessel, G.; Kootstra, F.; Kovalenko, A.; Krykunov, M. V.; van Lenthe, E.; McCormack, D. A.; Michalak, A.; Mitoraj, M.; Morton, S. M.; Neugebauer, J.; Nicu, V. P.; Noodleman, L.; Osinga, V. P.; Patchkovskii, S.; Pavanello, M.; Philipsen, P. H. T.; Post, D.; Pye, C. C.; Ravenek, W.; Rodríguez, J. I.; Ros, P.; Schipper, P. R. T.; Schreckenbach, G.; Seldenthuis, J. S.; Seth, M.; Snijders, J. G.; Solà, M.; Swart, M.; Swerhone, D.; te Velde, G.; Vernooijs, P.; Versluis, L.; Visscher, L.; Visser, O.; Wang, F.; Wesolowski, T. A.; van Wezenbeek, E. M.; Wiesenekker, G.; Wolff, S. K.; Woo, T. K.; Yakovlev, A. L. *ADF2012, SCM, Theoretical Chemistry*; Vrije Universiteit, Amsterdam, The Netherlands, <http://www.scm.com>.
- (106) Fonseca Guerra, C.; van der Wijst, T.; Poater, J.; Swart, M.; Bickelhaupt, F. M. Adenine versus guanine quartets in aqueous solution: dispersion-corrected DFT study on the differences in π -stacking and hydrogen-bonding behavior. *Theor. Chem. Acc.* **2010**, *125*, 245.
- (107) Stasyuk, O. A.; Sedlak, R.; Fonseca Guerra, C.; Hobza, P. Comparison of the DFT-SAPT and Canonical EDA Schemes for the Energy Decomposition of Various Types of Noncovalent Interactions. *J. Chem. Theory Comput.* **2018**, *14*, 3440.
- (108) Del Bene, J. E.; Alkorta, I.; Elguero, J. Halogen Bonding Involving CO and CS with Carbon as the Electron Donor. *Molecules* **2017**, *22*, 1955.
- (109) Wolters, L. P.; Schyman, P.; Pavan, M. J.; Jorgensen, W. L.; Bickelhaupt, M. F.; Kozuch, S. The many faces of halogen bonding: a review of theoretical models and methods WIREs. *Comput. Mol. Sci.* **2014**, *4*, 523.
- (110) Ran, J.; Hobza, P. On the Nature of Bonding in Lone Pair- π -Electron Complexes: CCSD(T)/Complete Basis Set Limit Calculations. *J. Chem. Theory Comput.* **2009**, *5*, 1180.
- (111) Novotný, J.; Bazzi, S.; Marek, R.; Kozelka, J. Lone-pair- π interactions: analysis of the physical origin and biological implications. *Phys. Chem. Chem. Phys.* **2016**, *18*, 19472.
- (112) Kozelka, J. Lone Pair- π Interactions in Biological Systems: Occurrence, Function, and Physical Origin. *Eur. Biophys. J.* **2017**, *46*, 729.